

A study on correlation effects in two dimensional topological insulators

Y. Tada,¹ R. Peters,² M. Oshikawa,¹ A. Koga,³ N. Kawakami,² and S. Fujimoto²

¹*Institute for Solid State Physics, The University of Tokyo, Chiba 277-8581, Japan*

²*Department of Physics, Kyoto University, Kyoto 606-8502, Japan*

³*Department of Physics, Tokyo Institute of Technology, Tokyo 152-8551, Japan*

We investigate correlation effects in two dimensional topological insulators (TI). In the first part, we discuss finite size effects for interacting systems of different sizes in a ribbon geometry. For large systems, there are two pairs of well separated massless modes on both edges. For these systems, we analyze the finite size effects using a standard bosonization approach. For small systems, where the edge states are massive Dirac fermions, we use the inhomogeneous dynamical mean field theory (DMFT) combined with iterative perturbation theory as an impurity solver to study interaction effects. We show that the finite size gap in the edge states is renormalized for weak interactions, which is consistent with a Fermi-liquid picture for small size TIs. In the second part, we investigate phase transitions in finite size TIs at zero temperature focusing on the effects of possible inter-edge Umklapp scattering for the edge states within the inhomogeneous DMFT using the numerical renormalization group. We show that correlation effects are effectively stronger near the edge sites because the coordination number is smaller than in the bulk. Therefore, the localization of the edge states around the edge sites, which is a fundamental property in TIs, is weakened for strong coupling strengths. However, we find no signs for "edge Mott insulating states" and the system stays in the topological insulating state, which is adiabatically connected to the non-interacting state, for all interaction strengths smaller than the critical value. Increasing the interaction further, a nearly homogeneous Mott insulating state is stabilized.

PACS numbers: Valid PACS appear here

I. INTRODUCTION

Topological insulators (TI) and topological superconductors (TSC) have been attracting great interest since the theoretical studies on the quantum spin Hall effect,¹⁻⁵ and their experimental realization.⁶⁻⁹ They can be characterized by an energy gap in the bulk and gapless edge or surface states at their boundaries.^{10,11} The direct relation between the bulk gap and the edge states, which is called the bulk-edge correspondence, is considered to be one of the most important properties in TIs and TSCs. These edge states are protected by topological properties of the bulk system, and are therefore robust against perturbations such as disorder or interactions which do not break the symmetries of the system.^{12,13} This suggests that, as long as the bulk remains gapful with non-trivial topology, the edge states exist at its boundaries. Correspondingly, in non-interacting systems, topological quantum phase transitions between topologically trivial and non-trivial phases require that the bulk gap is continuously closed. These gapped non-interacting systems which support the bulk-edge correspondence can be classified by ten distinct classes depending on their symmetries.¹⁴⁻¹⁶

However, it is not clear to what extent the bulk-edge correspondence holds in the presence of interactions. Interactions are expected to create novel correlated topological states,¹⁷⁻²⁸ such as TIs/TSCs *without* edge or surface states. For example, it has been proposed that strong correlations could realize a topologically non-trivial state without edge states when interactions become large.¹⁸ In this scenario, additional "zeros" in the Green's functions develop inside the bulk gap and finally

merge with the poles which correspond to the edge states. Thus, the resulting state does not possess any edge states although it remains gapped in the bulk. Among the models exhibiting topological insulating states, the Kane-Mele-Hubbard models have been extensively studied and the obtained phase diagrams show that the TI states extend to a wide region.¹⁹⁻²⁴ For large values of the Hubbard interaction U , magnetic states related to the honeycomb lattice structure are stabilized. In between, a possible realization of topological states without edge states has been proposed.²³ Correlation effects have also been investigated in one dimensional systems.²⁶⁻²⁸ It has been shown that, in time-reversal symmetric TSCs with inter-chain interactions, the ground states are characterized by fermion parity in addition to the time-reversal symmetry. These symmetries can distinguish different topological states and the ground states are labeled by topological numbers in \mathbb{Z}_8 instead of \mathbb{Z} for non-interacting systems. Furthermore, it was pointed out that in some cases the edge states actually disappear as interactions are increased without any gap closing.

Besides the possible realization of novel states in TIs and TSCs, strong interactions affect their quantitative properties. This is also the case for finite size systems, where the topological character would be smeared. Actually, it was pointed out that the edge states can be gapped due to tunneling processes between the two sides of the sample, and physical properties strongly depend on external parameters such as temperature and magnetic fields.²⁹⁻³² Finite size effects have been investigated also in the context of dimensional crossovers.³³⁻³⁷ However, finite size effects in the presence of interactions are still

not well understood, and properties of finite size TIs and TSCs would be sensitive to interactions in addition to external parameters. Moreover, correlation effects between the two sides of the system could have significant scattering processes which might lead to novel inter-edge correlated states.^{38–41}

In this article we discuss correlation effects in two dimensional topological insulators in a ribbon geometry at zero temperature. In the first part, we discuss finite size effects in interacting TIs which generate a gap in the edge states.^{29–37} For large systems with $L_y \gg \xi_{\text{TI}}$, where L_y is a width of the system and ξ_{TI} is a characteristic localization length of the edge states, the massless edge states at each side are well defined and can be described by Tomonaga-Luttinger liquids (TLL).^{38–41} We study effects of electron tunneling between the two edges by the standard bosonization method, and evaluate the finite size gap in spin and charge sectors.

Next, we concentrate on relatively small systems, for which the edge states are massive Dirac fermions. For this purpose we use the inhomogeneous dynamical mean field theory (DMFT)^{42–53} with the iterated perturbation theory (IPT) as an impurity solver.^{54,55} To be concrete, we analyze a Hamiltonian which has a topological non-trivial kinetic term as proposed for the HgTe/CdTe quantum wells and include an additional local Hubbard interaction. We show that the finite size gap is renormalized by interactions, which can be naturally understood based on a Fermi-liquid picture.

In the second part of this article, we discuss the paramagnetic Mott transition within the inhomogeneous DMFT using the numerical renormalization group (NRG)^{56,57} as an impurity solver. We show that correlation effects are significantly stronger near the edge sites, because the coordination number is smaller at the edges than in the bulk, as has been discussed in correlated systems without bulk gaps.^{43–49,58} Therefore, especially near the Mott transition, the localization of the edge states around the edge sites which is a fundamental property in TIs is weakened. However, possible inter-edge Umklapp scattering due to finite size effects does not seem to be important, and the "edge Mott insulating states" are not found. We show that even with strong correlations the ground state is a topological insulating state possessing edge states, which is adiabatically connected from the non-interacting system for all interaction strengths smaller than the critical value. When the interaction is stronger than the critical value, a nearly homogeneous Mott insulating state is stabilized. This is due to quantum tunneling of the electrons from the bulk to the edges, which was previously discussed in correlated metals. Finally, in the appendix of the article we present details on the NRG calculations.

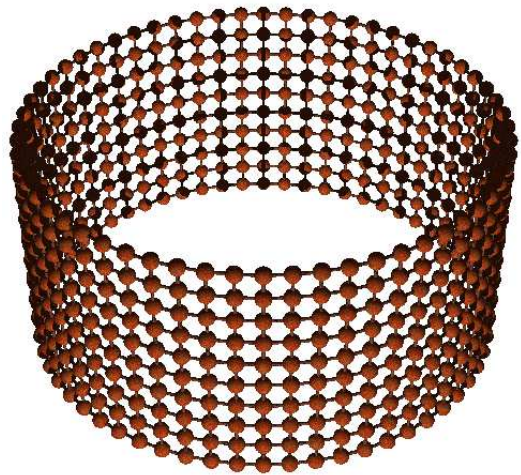


FIG. 1: (Color online) Ribbon geometry: square lattice with open boundaries in y -direction.

II. FINITE SIZE EFFECTS

In this section, we discuss finite size effects,^{29–37} in two dimensional TIs of different sizes in the ribbon geometry, see Fig. 1. When its width L_y is large compared to the characteristic localization length of the edge states, $L_y \gg \xi_{\text{TI}}$, the edge states, which are localized on the two sides, are well separated. Therefore, we can focus only on them and study correlation effects by using the standard bosonization technique. In this approach, forward scattering which has infrared singularities is fully taken into account, while other interaction terms are perturbatively treated. We note that this consideration is based on the bulk-edge correspondence, which allows us to forget the details of the bulk of the system.

For small system size where $L_y \gg \xi_{\text{TI}}$ is not satisfied, the tunneling between the two sides is no longer a perturbation and the edge states are massive Dirac fermions. In this case, we take into account electron correlations by means of the inhomogeneous DMFT for a Hubbard model which will be introduced later.

We first discuss relatively large size TIs in the next section, which is followed by the discussion of small systems in section II B.

A. Large systems: bosonization approach

It is known that in the presence of interactions, each of the edge states, which are localized at the two sides, can be described in terms of the helical Tomonaga-Luttinger liquid (HTLL).^{12,13} However, when the two sides are correlated, the edge states are usual Tomonaga-Luttinger liquids (TLL) with spin-charge separation.^{38–41} In this section, we investigate large size TIs by means of the standard bosonization approach,^{59,60} focusing on inter-edge tunneling processes.

Fermion operators for the edge states, localized at the edges $j = 1, 2$, are expressed as

$$\Psi_{jr\sigma}(x) = e^{irk_F x} \psi_{jr\sigma}(x)$$

for left ($r = -$ or L) and right ($r = +$ or R) movers with pseudo spins $\sigma = \uparrow, \downarrow$, and k_F being the Fermi wavenumber of the edge states. The effective Hamiltonian for the two edge states is given by

$$\begin{aligned} H &= H_1 + H_2 + H_{ch} + H_f + H_{f'} + H_{f''} + H', \\ H_1 &= -iv \int dx [\psi_{1R\uparrow}^\dagger \partial_x \psi_{1R\uparrow} - \psi_{1L\downarrow}^\dagger \partial_x \psi_{1L\downarrow}], \\ H_2 &= +iv \int dx [\psi_{2L\uparrow}^\dagger \partial_x \psi_{2L\uparrow} - \psi_{2R\downarrow}^\dagger \partial_x \psi_{2R\downarrow}], \\ H_{ch} &= g_{ch} \int dx [\rho_{1R\uparrow} \rho_{1R\uparrow} + \rho_{1L\downarrow} \rho_{1L\downarrow} + (1 \rightarrow 2)], \\ H_f &= g_f \int dx [\rho_{1R\uparrow} \rho_{1L\downarrow} + \rho_{2L\uparrow} \rho_{2R\downarrow}], \\ H_{f'} &= g_{f'} \int dx [\rho_{1R\uparrow} \rho_{2L\uparrow} + \rho_{1L\downarrow} \rho_{2R\downarrow}], \\ H_{f''} &= g_{f''} \int dx [\rho_{1R\uparrow} \rho_{2R\downarrow} + \rho_{1L\downarrow} \rho_{2L\uparrow}], \end{aligned}$$

where $\rho_{jr\sigma} = \psi_{jr\sigma}^\dagger \psi_{jr\sigma}$ and v is the Fermi velocity for the edge states. $H_{1,2}$ are kinetic terms for the edge states localized on edge-1 and edge-2 in the ribbon geometry, $H_{ch} \sim H_{f''}$ are forward scattering terms, and H' includes other scattering processes. In the terminology of usual spin 1/2 fermions on a chain, H_{ch} , H_f , $H_{f'}$, and $H_{f''}$ correspond to $g_{4\parallel}$, $g_{2\perp}$, $g_{2\parallel}$, and $g_{4\perp}$ terms, respectively. We note that, in the present study, SU(2) symmetry for spins is not required, and generally $g_f \geq g_{f'}, g_{f''}$ holds. Although the indices R/L are redundant, we keep them so that the relation between the usual spin 1/2 fermions and the present system is clear. We also note that the parameters in the above Hamiltonian should be regarded as those including correlation effects in the bulk system from which the effective one dimensional model is deduced.

Possible scattering processes in H' are

$$\begin{aligned} H' &= H_\lambda + H_{\lambda'} + H_{hf} + H_{sf} + H_{ef} + H_u + H_{u'}, \\ H_\lambda &= \lambda \int dx [\psi_{1R\uparrow}^\dagger \psi_{2L\uparrow} e^{-i2k_F x} + \psi_{2R\downarrow}^\dagger \psi_{1L\downarrow} e^{-i2k_F x} + (\text{h.c.})], \\ H_{\lambda'} &= \lambda' \int dx [\psi_{1R\uparrow}^\dagger \psi_{2R\downarrow} - \psi_{1L\downarrow}^\dagger \psi_{2L\uparrow} + (\text{h.c.})], \\ H_{hf} &= g_{hf} \int dx [\psi_{1R\uparrow}^\dagger \psi_{2R\downarrow}^\dagger \psi_{1L\downarrow} \psi_{2L\uparrow} e^{-i4k_F x} + \psi_{2L\uparrow}^\dagger \psi_{1L\downarrow}^\dagger \psi_{2R\downarrow} \psi_{1R\uparrow} e^{+i4k_F x}], \\ H_{ef} &= g_{ef} \int dx [\psi_{2L\uparrow}^\dagger \psi_{2R\downarrow}^\dagger \psi_{1L\downarrow} \psi_{1R\uparrow} + \psi_{1R\uparrow}^\dagger \psi_{1L\downarrow}^\dagger \psi_{2R\downarrow} \psi_{2L\uparrow}], \\ H_{sf} &= g_{sf} \int dx [\psi_{2L\uparrow}^\dagger \psi_{1R\uparrow}^\dagger \psi_{1L\downarrow} \psi_{2R\downarrow} + \psi_{2R\downarrow}^\dagger \psi_{1L\downarrow}^\dagger \psi_{1R\uparrow} \psi_{2L\uparrow}], \\ H_u &= g_u \int dx [\psi_{1R\uparrow}^\dagger(x) \psi_{1R\uparrow}^\dagger(x+a_0) \psi_{1L\downarrow}(x+a_0) \psi_{1L\downarrow}(x) e^{-i4k_F x} + \psi_{2L\uparrow}^\dagger \psi_{2L\uparrow}^\dagger \psi_{2R\downarrow} \psi_{2R\downarrow} e^{+i4k_F x} + (\text{h.c.})], \\ H_{u'} &= g_{u'} \int dx [\psi_{1R\uparrow}^\dagger(x) \psi_{1R\uparrow}^\dagger(x+a_0) \psi_{2L\uparrow}(x+a_0) \psi_{2L\uparrow}(x) e^{-i4k_F x} + \psi_{2R\downarrow}^\dagger \psi_{2R\downarrow}^\dagger \psi_{1L\downarrow} \psi_{1L\downarrow} e^{-i4k_F x} + (\text{h.c.})], \end{aligned}$$

where a_0 is the lattice constant. H_λ is a spin-conserving tunneling term, and $H_{\lambda'}$ is a spin-flip tunneling term which can be nonzero if the bulk Hamiltonian does not have the spin rotation symmetry. H_{hf} , H_{ef} , and H_{sf} describe "helicity-flip", "edge-flip" and "spin-flip" processes, respectively. H_u and $H_{u'}$ are Umklapp terms. H_{hf} , H_{ef} and $H_{u'}$ correspond to $g_{3\perp}$, $g_{1\perp}$ and $g_{3\parallel}$ terms in the spin 1/2 fermions. Obviously, they are invariant under the time-reversal transformation $\psi_{jR/L\uparrow}(x) \rightarrow \psi_{jL/R\downarrow}(x)$ and $\psi_{jR/L\downarrow}(x) \rightarrow -\psi_{jL/R\uparrow}(x)$.

To investigate the effects of H' , we use the standard bosonization approach.^{59,60} Bosonization relations are

$$\psi_{jr\sigma} = \frac{U_{jr\sigma}}{\sqrt{2\pi a_0}} e^{-ir\phi_{jr\sigma}},$$

where $U_{jr\sigma}$ are the Klein factors. We introduce

$$\begin{aligned}\phi_c &= (\phi_{1L\downarrow} + \phi_{1R\uparrow} + \phi_{2L\uparrow} + \phi_{2R\downarrow})/2\sqrt{2}, \\ \theta_c &= (\phi_{1L\downarrow} - \phi_{1R\uparrow} + \phi_{2L\uparrow} - \phi_{2R\downarrow})/2\sqrt{2}, \\ \phi_s &= (-\phi_{1L\downarrow} + \phi_{1R\uparrow} + \phi_{2L\uparrow} - \phi_{2R\downarrow})/2\sqrt{2}, \\ \theta_s &= (-\phi_{1L\downarrow} - \phi_{1R\uparrow} + \phi_{2L\uparrow} + \phi_{2R\downarrow})/2\sqrt{2}.\end{aligned}$$

These variables satisfy

$$[\phi_\mu(x), \partial\theta_\nu(y)] = i\pi\delta_{\mu\nu}\delta(x-y),$$

and the canonical momentum is $\Pi_\mu = (1/\pi)\partial\theta_\mu$.

Then, the kinetic term in the Hamiltonian $H_K = H_1 + H_2 + H_{ch} + H_f + H_{f'} + H_{f''}$ can be diagonalized and the bosonized Hamiltonian is,

$$\begin{aligned}H_K &= H_c + H_s, \\ H_c &= \frac{v_c}{2\pi} \int dx \left[\frac{1}{K_c} (\partial\phi_c)^2 + K_c (\partial\theta_c)^2 \right], \\ H_s &= \frac{v_s}{2\pi} \int dx \left[\frac{1}{K_s} (\partial\phi_s)^2 + K_s (\partial\theta_s)^2 \right],\end{aligned}$$

where

$$\begin{aligned}v_c &= [(v + \bar{g}_{ch} + \bar{g}_{f''} + \bar{g}_f + \bar{g}_{f'}) \\ &\quad \times (v + \bar{g}_{ch} + \bar{g}_{f''} - \bar{g}_f - \bar{g}_{f'})]^{1/2}, \\ K_c &= \left[\frac{v + \bar{g}_{ch} + \bar{g}_{f''} - \bar{g}_f - \bar{g}_{f'}}{v + \bar{g}_{ch} + \bar{g}_{f''} + \bar{g}_f + \bar{g}_{f'}} \right]^{1/2}, \\ v_s &= [(v + \bar{g}_{ch} - \bar{g}_{f''} + \bar{g}_f - \bar{g}_{f'}) \\ &\quad \times (v + \bar{g}_{ch} - \bar{g}_{f''} - \bar{g}_f + \bar{g}_{f'})]^{1/2}, \\ K_s &= \left[\frac{v + \bar{g}_{ch} - \bar{g}_{f''} + \bar{g}_f - \bar{g}_{f'}}{v + \bar{g}_{ch} - \bar{g}_{f''} - \bar{g}_f + \bar{g}_{f'}} \right]^{1/2},\end{aligned}$$

with $\bar{g}_{ch} = g_{ch}/\pi$ and $\bar{g} = g/2\pi$ for the other terms. H_c and H_s describe collective charge and spin excitations, respectively. As mentioned above, because $g_f \geq g_{f'}$, K_s is not fixed to unity and generally $K_s \geq 1$. If all the inter-edge correlated terms are neglected, H_c and H_s are essentially identical, and the edge states are nothing but two copies of the HTLL localized at each edge. We note that, if the bulk system is simply renormalized by a renormalization factor z in the presence of interactions, v is proportional to z and \bar{g} is to z^2 . Therefore, deviation of $K_{s,c}$ from unity would be suppressed by a factor z .

H' is also bosonized as

$$\begin{aligned}H_\lambda &= \frac{i\lambda}{\pi a_0} U_{1R\uparrow} U_{2L\uparrow} \int dx \sin(\sqrt{2}(\phi_c + \phi_s) - 2k_F x) + \frac{i\lambda}{\pi a_0} U_{2R\downarrow} U_{1L\downarrow} \int dx \sin(\sqrt{2}(\phi_c - \phi_s) - 2k_F x), \\ H_{\lambda'} &= \frac{i\lambda'}{\pi a_0} U_{2L\uparrow} U_{1L\downarrow} \int dx \sin \sqrt{2}(\phi_s + \theta_s) + \frac{i\lambda'}{\pi a_0} U_{1R\uparrow} U_{2R\downarrow} \int dx \sin \sqrt{2}(\phi_s - \theta_s), \\ H_{hf} &= -u \frac{2g_{hf}}{(2\pi a_0)^2} \int dx \cos(\sqrt{8}\phi_c - 4k_F x), \\ H_{ef} &= u \frac{2g_{ef}}{(2\pi a_0)^2} \int dx \cos \sqrt{8}\phi_s, \\ H_{sf} &= -u \frac{2g_{sf}}{(2\pi a_0)^2} \int dx \cos \sqrt{8}\theta_s, \\ H_u &= \frac{2g_u}{(2\pi a_0)^2} \int dx [\cos(\sqrt{8}(\phi_c + \theta_s) - 4k_F x) + \cos(\sqrt{8}(\phi_c - \theta_s) - 4k_F x)], \\ H_{u'} &= \frac{2g_{u'}}{(2\pi a_0)^2} \int dx [\cos(\sqrt{8}(\phi_c + \phi_s) - 4k_F x) + \cos(\sqrt{8}(\phi_c - \phi_s) - 4k_F x)],\end{aligned}$$

where $u = U_{2R\downarrow} U_{1R\uparrow} U_{1L\downarrow} U_{2L\uparrow}$. H_λ and Umklapp terms mix the charge and spin sectors.

The tunneling Hamiltonian H_λ includes $2k_F$ -oscillating factors, because it describes hybridizations between edge states on the two sides with the same wavenumber k . In the following, we focus on a special filling, $k_F = 0$, to evaluate the finite-size gap induced by the tunneling Hamiltonian. When $k_F = 0$, the chemical potential is exactly at the Dirac point of $H_{1,2}$ and all the oscillating factors in the Hamiltonian become unity $e^{i2k_F x} = e^{i4k_F x} = 1$. Then, we can evaluate the perturbations by looking at their scaling dimensions D_μ for H_μ ,

$$\begin{aligned} D_\lambda &= (K_c + K_s)/2, \\ D_{\lambda'} &= (K_s + 1/K_s)/2, \\ D_{hf} &= 2K_c, \\ D_{ef} &= 2K_s, \\ D_{sf} &= 2/K_s, \\ D_u &= 2(K_c + 1/K_s), \\ D_{u'} &= 2(K_c + K_s). \end{aligned}$$

From these equations, one sees that D_λ is the smallest scaling dimension around the non-interacting point $K_c = K_s = 1$, and therefore, the spin-conserving tunneling H_λ would be the most relevant perturbation in H' . Therefore, the edge states become gapped by H' , and they are no longer the TLL in finite size systems when $k_F \sim 0$. We note that, since the tunneling terms H_λ and $H_{\lambda'}$ have non-zero conformal spins, they contribute to renormalization group flows of H_{hf} , H_{ef} and H_{sf} , resulting in complicated flows.^{59–63} However, because H_λ is the most relevant perturbation, we focus only on H_λ and, in the following, simply neglect all the other perturbation terms in H' .

Under this approximation, we can estimate the finite size gap by using the standard analysis.⁵⁹ When λ is negative and large enough, conditions $\sqrt{2}(\phi_c \pm \phi_s) \simeq \pi/2$ give the minimal energy and the Hamiltonian would become

$$\begin{aligned} H_\lambda &\simeq \frac{\lambda}{\pi a_0} 2(\phi_c + \phi_s)^2 + \frac{\lambda}{\pi a_0} 2(\phi_c - \phi_s)^2 \\ &= \frac{2\tilde{\lambda}}{(\pi a_0)^2} (\phi_c^2 + \phi_s^2), \end{aligned}$$

where $\tilde{\lambda} = 2\pi a_0 \lambda$. Here, we have used a representation of the Klein factors where $U_{1R\uparrow} U_{2L\uparrow} = U_{2R\downarrow} U_{1L\downarrow} = -i$ can be satisfied, like $U_{1R\uparrow} = \sigma_1 \otimes \sigma_1$, $U_{1L\downarrow} = 1 \otimes \sigma_2$, $U_{2R\downarrow} = \sigma_3 \otimes \sigma_1$, $U_{2L\uparrow} = \sigma_2 \otimes \sigma_1$, where $\{\sigma_i\}$ are the Pauli matrices. ϕ_c has been shifted by $\pi/2\sqrt{2}$. Then, the spin and charge sectors are decoupled and the gaps induced by H_λ are respectively evaluated as

$$\Delta_{s,c}^\lambda \sim w \left(\frac{K_{s,c} \tilde{\lambda}}{w} \right)^{1/(2-D_\lambda)},$$

where w is an effective band width of the edge states which would correspond to the bulk gap Δ_{TI} . $\Delta_{s,c}$ are

enhanced by the forward scattering. We stress that, even for the weak interactions $K_{s,c} \simeq 1$, both of the spin and charge sectors are gapped by the tunneling H_λ . Therefore, the TLL description fails for the low energy edge states in the finite size TIs when $k_F \simeq 0$. Nevertheless, correlation effects peculiar to one-dimensional systems appear as a difference between the charge gap and the spin gap, $\Delta_c^\lambda \neq \Delta_s^\lambda$, which characterizes the spin-charge separation. We stress that the charge gap can be much smaller than the spin gap in strongly correlated regions provided that the edge states can be treated as one-dimensional systems. It should be an interesting issue to experimentally detect the spin-charge separation raised by the one-dimensional correlation effect from the measurement of the Hall effect and the spin Hall effect which are governed by the edge states.

In the above derivation of $\Delta_{s,c}$, we have simply neglected other interaction terms in H' . However, they can be important in a strongly correlated regime where $K_{s,c}$ is away from unity. As mentioned above, $H_{\lambda'}$, H_{sf} , H_u describe spin flip processes which are difficult to take into account in numerical calculations. On the other hand, the inter-edge interactions H_{hf} , $H_{u'}$ are spin-conserving Umklapp terms and might lead to the possible "edge Mott insulating states". The effects of the inter-edge Umklapp scattering are discussed in Sec. III.

At the end, we note that all the parameters in the expressions for the gaps, $K_{s,c}$, $\tilde{\lambda}$ and w , are derived from the two dimensional bulk system and would be renormalized by the interactions in the bulk. This renormalization cannot be calculated from the one dimensional model, and rather should be included in the initial values of the parameters.

In the next section, we analyze small TIs by an alternative approach which is based on a Fermi-liquid picture for the TIs.

B. Small systems: DMFT+IPT calculations

When the system size is small enough so that the tunneling between the edges is no longer a small perturbation, analyses based on well-defined massless modes are not applicable anymore. In this section, we consider correlation effects in small size systems whose edge states are massive Dirac fermions.

To be concrete, we consider the following Hamiltonian defined on a square lattice in the ribbon geometry (Fig. 1),

$$H = H_{\text{BHZ}} + H_{\text{int}}, \quad (1)$$

where H_{BHZ} is topologically equivalent to the Hamiltonian for the HgTe/CdTe quantum wells.^{3,6,10,11} H_{int} is an interaction term between the electrons. The Hamiltonian contains two orbitals described by $C_i = (c_{i1\uparrow}, c_{i2\uparrow}, c_{i1\downarrow}, c_{i2\downarrow})^T$ where the indices 1, 2 (\uparrow, \downarrow) label orbitals (pseudo spins). The kinetic energy can be written as

$$H_{\text{BHZ}} = \sum_{ij} C_i^\dagger \hat{H}_{ij} C_j, \quad (2a)$$

$$\hat{H}_{ij} = \begin{bmatrix} \mathcal{H}_{ij} & 0 \\ 0 & \mathcal{H}_{ij}^* \end{bmatrix}, \quad (2b)$$

$$\mathcal{H}_{ij} = \begin{bmatrix} M_0 \delta_{ij} - t(\delta_{i,j+\hat{x}} + \delta_{i,j-\hat{x}}) & t'[\delta_{i,j+\hat{x}} - \delta_{i,j-\hat{x}} + \delta_{i,j+\hat{y}} - \delta_{i,j-\hat{y}}] \\ t'[i(\delta_{i,j+\hat{x}} - \delta_{i,j-\hat{x}}) + \delta_{i,j-\hat{y}} - \delta_{i,j+\hat{y}}] & -M_0 \delta_{ij} + t(\delta_{i,j+\hat{x}} + \delta_{i,j-\hat{x}}) \end{bmatrix}. \quad (2c)$$

The periodic boundary condition is imposed for the x -direction, while the system has a finite width L_y for the y -direction. As will be discussed later, this Hamiltonian is particle-hole symmetric when the filling is $n_1 + n_2 = 1$ per spin-direction. Regarding the interaction term, we consider the simplest Hamiltonian

$$H_{\text{int}} = U \sum_{il} n_{i\uparrow} n_{i\downarrow}, \quad (3)$$

where $n_{i\sigma} = c_{i\sigma}^\dagger c_{i\sigma}$. The total Hamiltonian is a Hubbard model with inter-site inter-orbital hopping t' corresponding to the spin-orbit (SO) interaction in the present article. In the following, we take t as the energy unit $t = 1$, and the SO interaction t' is fixed to be $t' = 0.25$. Furthermore, we set the filling to $n_{i1} + n_{i2} = 1$ per spin-direction for all sites. We also fix $L_y = 10$ and $M_0 = -1.0$, if not specified, for which the finite size gap is $\Delta_f \sim 0.1\Delta_{\text{TI}}$ in the absence of the interaction. As discussed in the previous section, in finite size TIs, infrared singularities are cut off and descriptions based on the TLL fail to capture gapped edge states when their Fermi wavenumber is small. Instead, a Fermi-liquid picture of correlated band insulators would give a correct understanding where the edge states are massive Dirac fermions, as will be discussed in the following sections.

1. Non-interacting case

Before discussing correlation effects, we want to show some basic properties of the non-interacting system. In Fig. 2, the dispersion relation for $M_0 = -1.0$ calculated from H_{BHZ} is shown. The dispersion is particle-hole symmetric and edge states exist for $0 < |M_0| < 4$. The bulk gap is $\Delta_{\text{TI}} \simeq 1.0$ corresponding to $t' = 0.25$. The edge states have a small but finite gap as discussed in previous studies,²⁹⁻³⁷ The finite-size gap Δ_f depends on the parameter M_0 and it is oscillating when M_0 is tuned as shown in Fig. 3 for $L_y = 10, 20$ and 40 . The number of the oscillation for $0 < |M_0| < 4$ is $2(L_y - 1)$, which is related to the number of the eigenstates of H_{BHZ} for a fixed k_x . This oscillation is specific to lattice systems, and we have to be careful about this when discussing correlation effects in the following sections where oscillations in Δ_f can also be seen. Oscillations in bulk gaps with respect to system sizes have been discussed in many articles

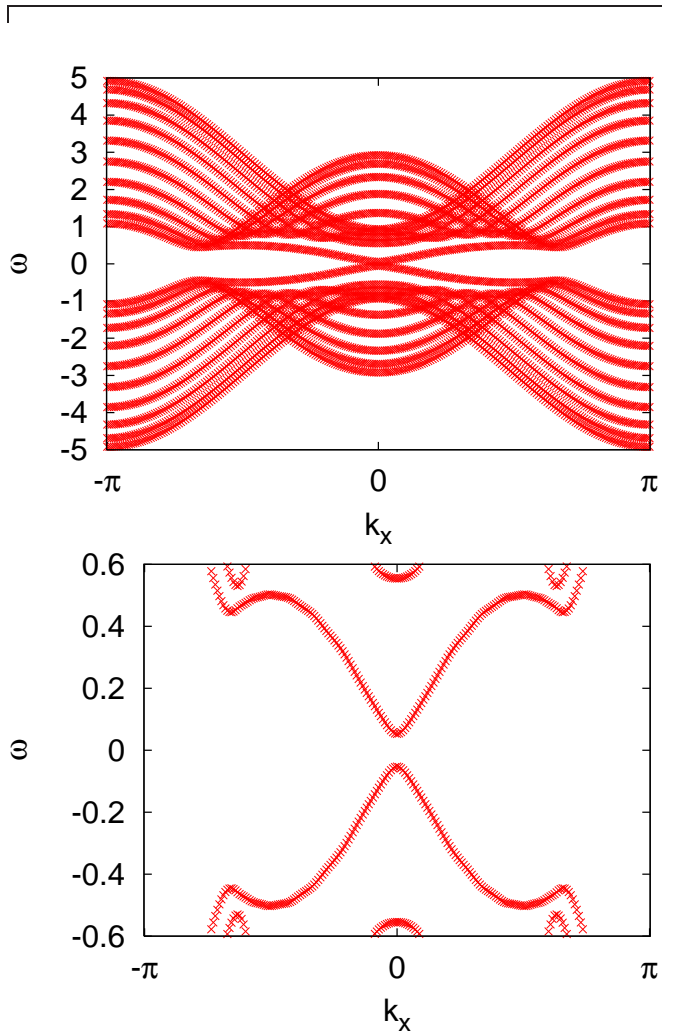


FIG. 2: (Color online) The dispersion relation for $M_0 = -1.0$. The edge states spectrum is enlarged in the lower panel so that the finite size gap can be seen.

and oscillatory dimensional crossovers are seen in some classes of TIs and TSCs.²⁹⁻³⁷ However, in our study, the non-interacting system remains topologically non-trivial as long as $0 < |M_0| < 4$. Δ_f is exponentially decreasing as L_y is increased, and its size dependence is roughly

$$\Delta_f \simeq \Delta_{f0} \exp\left(-L_y/\xi_{\text{TI}}^{(0)}\right),$$

$$\xi_{\text{TI}}^{(0)} \sim t'/M_0,$$

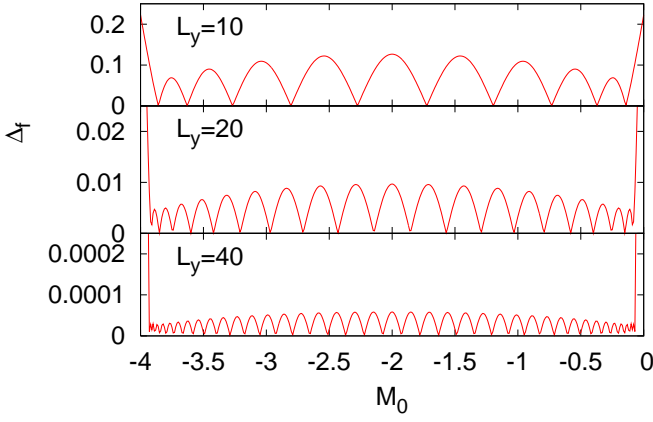


FIG. 3: (Color online) The finite size gap as a function of M_0 for $L_y = 10, 20, 40$ from the top to the bottom. For $0 < M_0 < 4$, Δ_f depends on M_0 in the same way as for $-4 < M_0 < 0$.

where $\xi_{\text{TI}}^{(0)}$ characterizes the localization of the edge states around the edge sites in the non-interacting system. Δ_{f0} is defined by a combination of the parameters in H_{BHZ} . Exact expressions for these quantities in the continuum limit can be found in Zhou et al.²⁹

Naive expectation based on the Fermi-liquid picture together with an assumption that in the presence of the interaction U the low energy states are renormalized by a single renormalization factor z , results in a finite-size gap

$$\Delta_{f0}(U) \simeq z \Delta_{f0}(U = 0), \quad (4a)$$

$$\xi_{\text{TI}}(U) \sim z t' / z M_0 \sim \xi_{\text{TI}}^{(0)}. \quad (4b)$$

Renormalizations of t' and M_0 would cancel out and $\xi_{\text{TI}}(U)$ would be equal to $\xi_{\text{TI}}^{(0)}$. Therefore, our simplest expectation is that the amplitude of the finite size gap is renormalized by z while ξ_{TI} is not, although the legitimacy of the above assumption is not so clear. In the following sections, we investigate correlation effects and show that the naive expectation actually holds in the presence of the Hubbard interaction within the DMFT.

2. Inhomogeneous DMFT+IPT

In this section, we discuss the correlation effects by means of the inhomogeneous DMFT+IPT. The inhomogeneous DMFT is an extension of the DMFT⁴² to inhomogeneous systems and has been applied to, e.g. metallic surfaces,^{44,45} heterostructures,⁴⁶⁻⁴⁹ and optical lattices.⁵⁰⁻⁵³ We note that, in the present study, the edge states for small L_y are massive and not the massless HTLLs as discussed in the previous sections. The whole two dimensional system including the edge degrees of freedom is supposed to be a gapped Fermi-liquid. Therefore, we expect that inhomogeneous DMFT can capture the main properties of the edge states in the presence of

interactions, although it is known that DMFT fails to describe the low energy TLL behavior in one dimension.⁶⁴

To calculate the selfenergy, we solve the following self consistent equations for $y = 1, 2, \dots, L_y$,

$$\mathcal{G}_{aa'}^{-1}(\omega, y) = \left[\frac{1}{L_x} \sum_{k_x} G(\omega, k_x, y, y) \right]_{aa'}^{-1} + \Sigma_{aa'}(\omega, y),$$

where $a = (l\sigma)$, \mathcal{G} is the cavity Green's function and L_x is the number of k_x points, which is taken to be sufficiently large. The lattice Green's function $G_{aa'}(\omega, k_x, y, y')$ is a $4L_y \times 4L_y$ matrix, where the system size is fixed as $L_y = 10$ in the present study. We note that G is spin-diagonal and $\sum_{k_x} G_{l\sigma, l'\sigma}(\omega, k_x, y, y) = \sum_{k_x} G_{l\bar{\sigma}, l'\bar{\sigma}}(\omega, k_x, y, y)$ is satisfied in our ribbon geometry, and therefore we often suppress the spin indices throughout this article.

The selfenergy of the effective impurity problem is calculated by means of the IPT which can compute the self-energy as a function of real frequency ω .^{54,55} Within the IPT, the selfenergy is evaluated in the following way: The first order contribution is $\Sigma_{l\sigma, l'\sigma}^{(1)}(y) = U n_{l\sigma}(y) \delta_{ll'} \delta_{\sigma\sigma'}$ where $n_{l\sigma}(y)$ is the electron density for orbital l and spin σ at site y . We note that $\sum_{l\sigma} n_{l\sigma}(y) = 1$ for all the sites. The second order is

$$\begin{aligned} \Sigma_{d_1 d_2}^{(2)}(\omega) &= -\frac{1}{2\pi^3} \Gamma_{d_2 b_2}^{a_1 c_1} \Gamma_{a_2 c_2}^{d_1 b_1} \\ &\times \int d\varepsilon d\varepsilon' d\varepsilon'' \text{Im} \tilde{\mathcal{G}}_{a_2 a_1}(\varepsilon) \text{Im} \tilde{\mathcal{G}}_{b_2 b_1}(\varepsilon') \text{Im} \tilde{\mathcal{G}}_{c_2 c_1}(\varepsilon'') \\ &\times \frac{1}{\omega - \varepsilon + \varepsilon' - \varepsilon''} \left\{ f(\varepsilon) [1 - f(\varepsilon')] f(\varepsilon'') \right. \\ &\left. + [1 - f(\varepsilon)] f(\varepsilon') [1 - f(\varepsilon'')] \right\}, \end{aligned}$$

where $a, b, c, d = (l\sigma)$ and Γ is an antisymmetric bare vertex. f is the Fermi distribution function. In the present model, $\Gamma_{l\sigma, l\bar{\sigma}}^{l\sigma, l\bar{\sigma}} = U$, $\Gamma_{l\sigma, l\bar{\sigma}}^{l\bar{\sigma}, l\sigma} = -U$, and all the other elements are zero. The Green's function $\tilde{\mathcal{G}}$ is given by $\tilde{\mathcal{G}}_{l\sigma, l'\sigma}^{-1} = \mathcal{G}_{l\sigma, l'\sigma}^{-1} - U n_{l\sigma} \delta_{ll'} \delta_{\sigma\sigma'}$. The selfenergy is interpolated from the weak coupling to the atomic and high energy limit in the IPT calculations,

$$\Sigma_{l\sigma, l'\sigma}(\omega) = \Sigma_{l\sigma, l'\sigma}^{(1)} + \frac{A_{ll'} \Sigma_{l\sigma, l'\sigma}^{(2)}(\omega)}{1 - B_{ll'} \Sigma_{l\sigma, l'\sigma}^{(2)}(\omega)},$$

where $A_{ll'} = \delta_{ll'} n_l (1 - n_l/2) / \tilde{n}_l (1 - \tilde{n}_l/2) + (1 - \delta_{ll'})$, $B_{ll'} = \delta_{ll'} 2(1 - n_l) / \tilde{n}_l (1 - \tilde{n}_l/2)$, and \tilde{n}_l is calculated from $\tilde{\mathcal{G}}$. We use a simplified scheme which has been successfully applied to correlated metals away from the half filling, in which the effective chemical potential is simply determined from $\Sigma(\omega = 0) = \Sigma^{(1)}(0)$.⁵⁵

In Figs. 4 and 5, we show the selfenergy and the local Green's functions for half of the system width for $U = 4$.

As will be discussed later, the local selfenergies for the other half are $\text{Im} \Sigma_{11,22}(\omega, L_y - y + 1) = \text{Im} \Sigma_{11,22}(\omega, y)$ and $\text{Im} \Sigma_{12,21}(\omega, L_y - y + 1) = -\text{Im} \Sigma_{12,21}(\omega, y)$. The

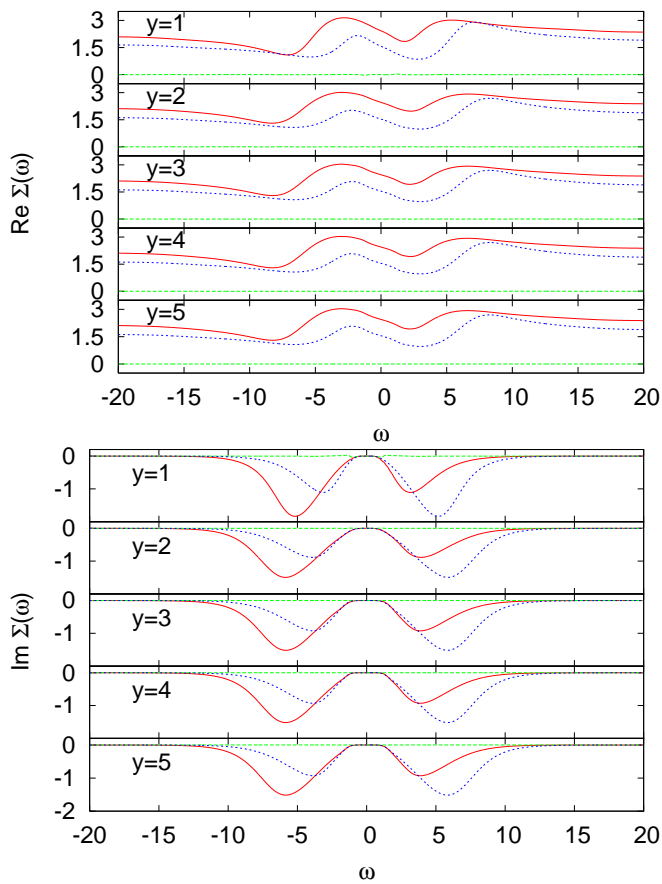


FIG. 4: (Color online) Selfenergy for $U = 4$ and $L_y = 10$. Red, green, blue curves are Σ_{11} , $\Sigma_{12,21}$ and Σ_{22} , respectively.

local Green's functions show the same symmetry properties. We see that, the diagonal elements of the selfenergy are similar to those of simple band insulators; e.g. $\text{Im}\Sigma_{11,22}(\omega)$ seem to have gap like structures. They behave like $\text{Im}\Sigma_{11,22}(\omega, y) \simeq -b(y)\omega^2$ for small ω , where the prefactors $b(y)$ are much smaller than those in metallic systems. This is because the density of states has only small weight around $\omega = 0$ which corresponds to the edge states. On the other hand, although $\text{Im}G_{12,21}$ is comparable to $\text{Im}G_{11,22}$ in magnitude at least for $y = 1$ around $\omega \sim \Delta_{\text{TI}}$, $\Sigma_{12,21}$ is much smaller than $\Sigma_{11,22}$. In Fig. 6, we also show the energy spectrum for $U = 4$ defined by $A(k_x, \omega) = -(1/L_y) \sum_y \text{Im}[G_{11}(k_x, y, \omega) + G_{22}(k_x, y, \omega)]$. Compared to Fig. 2, the edge states around $\omega = 0$ are renormalized and high energy structures are smeared. We note that, although the massive Dirac states are topologically protected, namely they are free from the single particle backscattering and the intra-edge Umklapp scattering in the spin conserved systems, they have a long but finite lifetime due to the forward scattering. A direct comparison with a non-perturbative impurity solver, the NRG, is shown in Appendix A 3.

The finite size gap Δ_f as a function of U can be calcu-

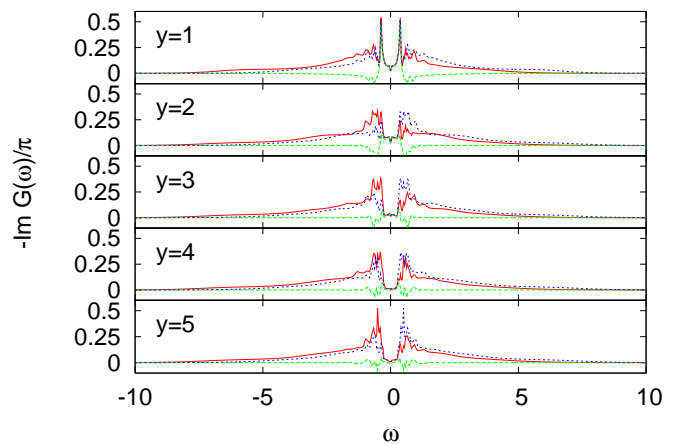


FIG. 5: (Color online) The local Green's functions for $y = 1 \sim 5$ from the top to the bottom when $U = 4$ and $L_y = 10$. The red, green, and blue curves are for G_{11} , $G_{12,21}$, and G_{22} , respectively.

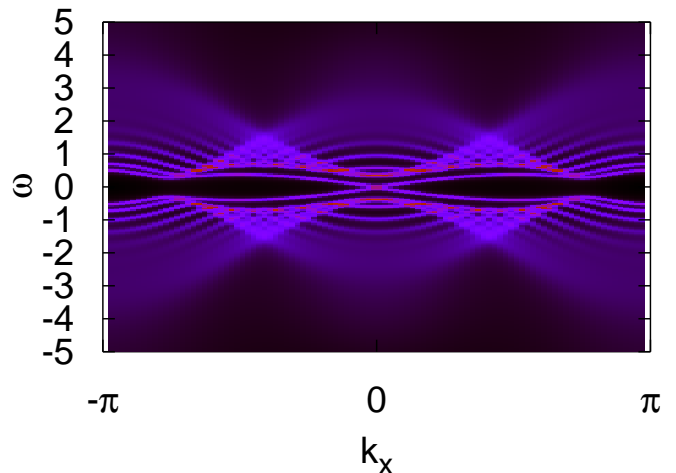


FIG. 6: (Color online) The energy spectrum $A(k_x, \omega)$ for $U = 4$ and $L_y = 10$.

lated from an effective Hamiltonian

$$\bar{H}(\omega) = \hat{H} + \Sigma(\omega).$$

For $|\omega| < \Delta_{\text{TI}}$, $\text{Im}\Sigma(\omega)$ is much smaller than that for $t' = 0$ and can be neglected when evaluating the finite size gap. We can identify the positions of zeros in $\omega - \bar{H}(\omega)$, which correspond to the energy eigenvalues of the edge states. As shown in the upper panel of Fig. 7, Δ_f is an oscillating function of U . This oscillation has its origin in the non-interacting system in Fig. 3, because constant terms in $\text{Re}\Sigma_{11,22}$ play the same role as M_0 in the inverse of the Green's functions. The bulk gap Δ_{TI} is simply estimated from the next lowest excitation energy of \bar{H} at $k_x = 0$, and $\mathcal{Z} = (1/L_y) \sum_y z(y)$ is also shown in the figure. We note that, compared to $\Delta_{\text{TI}}(U)$, the renormalization of Δ_f is rather moderate, because $z(y)$, which is defined by the derivative of Σ at $\omega = 0$, is larger than that at $\omega \simeq \Delta_{\text{TI}}$. To extract the correlation effects

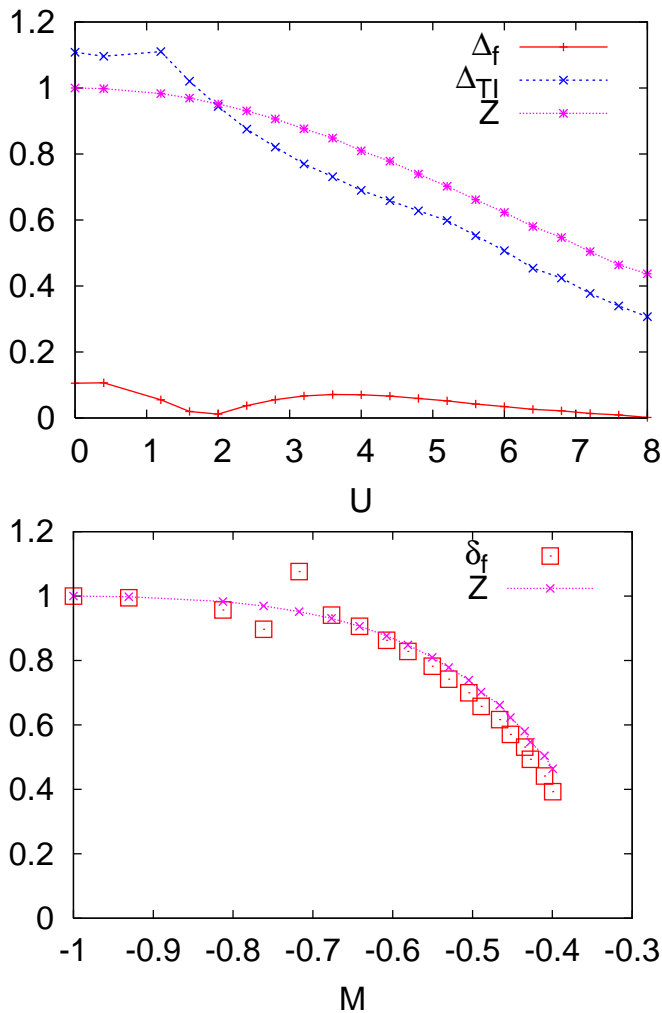


FIG. 7: (Color online) (Upper panel) The finite size gap Δ_f , the bulk gap Δ_{TI} , and the y -averaged renormalization factor \mathcal{Z} as functions of U for $L_y = 10$. (Lower panel) The ratio of the finite size gap δ_f and \mathcal{Z} as functions of \mathcal{M} .

from this oscillating Δ_f , we replot it as a function of a parameter \mathcal{M} corresponding to M_0 . We define

$$\mathcal{M}(U) = \mathcal{M}_0 + \frac{1}{2L_y} \sum_y \left[\text{Re}\Sigma_{11}(\omega = 0, y) - \text{Re}\Sigma_{22}(\omega = 0, y) \right],$$

$$\delta_f(\mathcal{M}) = \Delta_f(\mathcal{M}(U)) / \Delta_f(M_0; U = 0)|_{M_0 = \mathcal{M}},$$

where $\mathcal{M}_0 = -1.0$. In the definition of δ_f , we have identified the non-interacting parameter M_0 as \mathcal{M} . In the lower panel in Fig. 7, we show $\delta_f(\mathcal{M})$ and $\mathcal{Z}(\mathcal{M})$. We see that $\delta_f(\mathcal{M})$ and $\mathcal{Z}(\mathcal{M})$ well coincide, which means that our naive expectation Eqs. (4a) and (4b) based on the Fermi-liquid picture actually holds within the DMFT+IPT calculations. We note that, for weak interactions, site dependence in $\Sigma(y)$ is not strong and Δ_f can be well understood in terms of their averages, \mathcal{M} and \mathcal{Z} . If the site dependence in Σ is significant, this interpretation is not

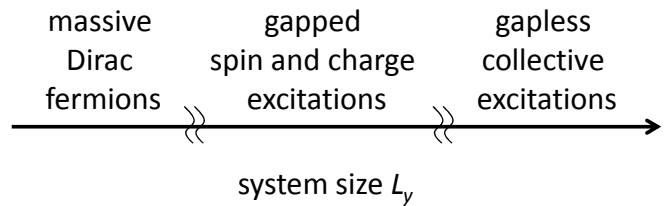


FIG. 8: The elementary excitations in two dimensional TIs for different system sizes when the Coulomb interactions are weak.

longer applicable.

In this section, we have discussed the correlation effects for small size systems, while the previous section was dedicated to rather large systems. For these two limiting situations, the physical pictures are very different; the edge states are renormalized massive Dirac fermions for small systems, instead of the gapped spin and charge collective modes for large systems. However, it would be possible to smoothly connect them to each other as the system size L_y is tuned. If one starts from a small size where the single particle spectrum has a gap, one should calculate the susceptibilities to see the gaps in the spin and charge collective excitations. These gaps in the susceptibilities should be evaluated with the vertex corrections being taken into account. Although such calculations are beyond the present DMFT calculations, a crossover would take place at some length scale of the system. Such crossovers between two or three dimensional physics and one dimensional physics with respect to energy scales are also seen in ladder systems.⁵⁹ In Fig. 8, we summarize the elementary excitations in two dimensional TIs for different system sizes when the Coulomb interactions are weak. In the limit $L_y \rightarrow \infty$ where the inter-edge correlation is negligible, the “gapless collective excitations” correspond to the HTLL.

III. MOTT TRANSITION

In this section, we discuss the paramagnetic Mott transition for a topologically nontrivial system by using the inhomogeneous DMFT. We use the same model Hamiltonian as in the previous section, Eq. (1), and suppress possible magnetic instabilities. In previous studies^{17,18,23,26–28} it was discussed that for TIs and TSCs with strong interactions novel ground states might be realized, in which the bulk remains gapped with a non-trivial topological number while the edge states are suppressed by interaction effects. Such states are called “edge Mott insulating states”, and can be explicitly defined in terms of the Green’s functions.¹⁸ Let us briefly consider a semi-infinite TI, which is built up as a heterostructure of the vacuum and the TI having one boundary. In the absence of interactions, poles are supposed to be in the Green’s functions corresponding to the edge states, while in the presence of interactions there might

be additional zeros as was discussed by Gurarie¹⁸. In the latter case, the edge states are suppressed and the ground state can be characterized as an “edge Mott insulating state”. Although this discussion cannot be directly applied to finite size systems with two boundaries, the selfenergy must have poles inside the bulk gap to realize the edge Mott insulating state, which characterizes the TIs with Mott insulating edge states. In this scenario, the finite size gap would be replaced by the Mott gap as interactions are increased. We note that, to obtain the edge Mott insulating states, the Umklapp scattering for the edge states is essential. Although, the Umklapp scattering of the edges at the same side is absent in our model, there are possible Umklapp scattering processes which involve both sides. In the edge state Hamiltonians introduced in Sec. II A these processes are given by H_{hf} and $H_{u'}$, while H_u is absent. Such scattering processes might drive the edge states into a Mott insulating state, keeping the bulk a topological insulator. We note that, while $H_{u'}$ is characterized by scattering at different sites, H_{hf} describes scattering at a single site. Because there is some overlap of the edge state wave functions which are localized mainly at opposite sides, effects of H_{hf} are taken into account within the inhomogeneous DMFT. In addition, when $\Delta_f/\Delta_{\text{TI}}$ is not so small and U is large compared to Δ_{TI} , the inter-edge Umklapp scattering is expected to be important.

A. Symmetries in Green’s function and selfenergy

Before discussing results obtained with inhomogeneous DMFT, we discuss some identity relations in G and Σ arising from the particle-hole symmetry in the Hamiltonian Eq. (1). These identities are quite useful for checking numerical results and simplifying calculations, thus improving the accuracy.

The particle-hole transformation, defined by a unitary operator \mathcal{C} , is given as

$$\begin{aligned} c_{i1\sigma} &\rightarrow c_{i2\sigma}^\dagger, \\ c_{i2\sigma} &\rightarrow c_{i1\sigma}^\dagger. \end{aligned}$$

The condition that the Hamiltonian should be invariant under this transformation determines the chemical potential. The interaction in the model is given by $H_{\text{int}} = U \sum_{i\ell} n_{i\ell\uparrow} n_{i\ell\downarrow}$. Thus, the chemical potential should be $\mu = U/2$ so that particle-hole symmetry is conserved. We note that our model belongs to the class DIII-Hamiltonians which describe the $p \pm ip$ superconductors,^{14–16} such as the Rashba superconductors,⁶⁵ if we identify our particle-hole symmetry \mathcal{C} as emergent particle-hole symmetry in superconductors.²⁸ This correspondence would allow us to interpret the off-diagonal selfenergy $\Sigma_{12,21}$ as an anomalous selfenergy of the superconductivity if the emergent particle-hole symmetry is kept in the presence of interactions.

From the particle hole symmetry we can directly derive identities in $G(\omega)$ and $\Sigma(\omega)$. The local retarded Green’s function for site i satisfies

$$\begin{bmatrix} G_{11}^R(\omega, i) & G_{12}^R(\omega, i) \\ G_{21}^R(\omega, i) & G_{22}^R(\omega, i) \end{bmatrix} = \begin{bmatrix} -G_{22}^R(-\omega, i)^* & -G_{12}^R(-\omega, i)^* \\ -G_{21}^R(-\omega, i)^* & -G_{11}^R(-\omega, i)^* \end{bmatrix}. \quad (5)$$

We note that the inverse of the matrix $G(\omega) = [G_{ll'}(\omega, i, j)]$ also satisfies the corresponding relations, since $G(\omega)^{-1} \cdot G(\omega) = G(\omega) \cdot G(\omega)^{-1} = \mathbf{1}$.

Thus, the selfenergy for a fixed filling fulfills similar relations, which are directly derived from

$$\begin{aligned} \Sigma^R(\mu; \omega, i) &= [G_0^R(\mu; \omega)]_{ii}^{-1} - [G^R(\mu; \omega)]_{ii}^{-1} \\ &= [[G_0^R(\mu; \omega)]_{ii}^{-1} - [G^R(\mu_0; \omega)]_{ii}^{-1}] + (\mu - \mu_0), \end{aligned}$$

where each of the non-interacting and interacting local Green’s functions, the site-diagonal elements of the matrices $G_0^R(\mu_0; \omega)$ and $G^R(\mu; \omega)$, satisfies Eq.(5). The chemical potential is $\mu_0 = 0$ and $\mu = U/2$. Therefore, the local selfenergy should satisfy

$$\begin{aligned} &\begin{bmatrix} \Sigma_{11}^R(-\omega, i) - \mu & \Sigma_{12}^R(-\omega, i) \\ \Sigma_{21}^R(-\omega, i) & \Sigma_{22}^R(-\omega, i) - \mu \end{bmatrix} \\ &= \begin{bmatrix} -\Sigma_{22}^R(\omega, i)^* + \mu & -\Sigma_{12}^R(\omega, i)^* \\ -\Sigma_{21}^R(\omega, i)^* & -\Sigma_{11}^R(\omega, i)^* + \mu \end{bmatrix}. \quad (6) \end{aligned}$$

We see that the real part of $\Sigma_{12,21}(\omega)$ is an odd function of ω and the imaginary part is an even function, and especially $\text{Re}\Sigma_{12,21}(\omega = 0) = 0$. Looking at the inverse of the Green’s function $G^{-1} = [\omega - \hat{H} - \Sigma]$, the off-diagonal selfenergy $\Sigma_{12,21}(\omega, i)$ can be interpreted as a local hybridization between the orbitals, which does not add to the inter-site inter-orbital hopping t' in the Hamiltonian H . In this interpretation, $\Sigma_{12,21}(\omega, y)$ are regarded as the induced “ s -wave” hybridization between the orbitals arising from the “ p -wave” hybridization between the orbitals arising from the on-site interaction.⁶⁶ The odd frequency dependence in $\text{Re}\Sigma_{12,21}(\omega)$ is related to the odd parity character of the inter-orbital hopping t' .

The odd parity $\Sigma_{12,21}$ in our system is in contrast to those in trivial band insulators, where inter-orbital hopping is local, s -wave-like. It can be shown for this model that off-diagonal elements behave like $\Sigma_{12}(\omega, i) = \Sigma_{12}(-\omega, i)^*$. Therefore, $\text{Re}\Sigma_{12,21}(\omega = 0, i) \neq 0$ can add to the local hybridization, which suggests that the bulk gap grows continuously as U is increased. This has been shown in the previous studies for topologically trivial correlated band insulators.^{67–69} In the context of superconductivity, this would correspond to the BCS-BEC crossover for the s -wave pairing states.^{70,71}

We also note that this argument can easily be generalized to the non-local selfenergy, and the off-diagonal elements in the present model satisfy $\Sigma_{12}(\omega, i, j) = -\Sigma_{12}(-\omega, j, i)^*$ for sites i, j . At $\omega = 0$, $\Sigma_{12}(0, i, j)$ has the same symmetry as the inter-site inter-orbital hopping and enhances it. We again stress that the odd-parity symmetries in the off-diagonal selfenergy are characteristic of our model. However, constant terms in

$\text{Re}\Sigma_{12}(\omega, i, j)$ do not appear in the lowest order in U , and $\text{Re}\Sigma_{12}(0, i, j)$ comes only from higher order terms in U . Although $\text{Re}\Sigma_{12}(0, i, j)$ is expected to be small in the present model, sufficiently large $\text{Re}\Sigma_{12}(0, i, j)$ might lead to a crossover with continuous growth of the bulk gap in the presence of on-site interactions. However, previous studies on the Kane-Mele Hubbard model taking into account spatial correlations show a renormalization of the bulk gap,²⁴ which implies that in our model $\Sigma_{12}(0, i, j)$ for $i \neq j$ is not dominant, too.

Other relations in G and Σ corresponding to an inversion transformation along the y -axis also exist. The inversion transformation \mathcal{I} is defined by

$$c_{i\sigma} \rightarrow c_{\bar{i}\sigma},$$

where $\bar{i} = (-x, L_y + 1 - y)$. Under this transformation, the Hamiltonian satisfies $\mathcal{I}H(t_{ij}^{11,22}, t_{ij}^{12,21})\mathcal{I}^{-1} = H(t_{ij}^{11,22}, -t_{ij}^{12,21})$. Because $G_{11,22}$ are even with respect to $t_{12,21}$ while $G_{12,21}$ are odd, the following relations hold:

$$\begin{bmatrix} G_{11}^R(\omega, i) & G_{12}^R(\omega, i) \\ G_{21}^R(\omega, i) & G_{22}^R(\omega, i) \end{bmatrix} = \begin{bmatrix} G_{11}^R(\omega, \bar{i}) & -G_{12}^R(\omega, \bar{i}) \\ -G_{21}^R(\omega, \bar{i}) & G_{22}^R(\omega, \bar{i}) \end{bmatrix}, \quad (7)$$

$$\begin{bmatrix} \Sigma_{11}^R(\omega, i) & \Sigma_{12}^R(\omega, i) \\ \Sigma_{21}^R(\omega, i) & \Sigma_{22}^R(\omega, i) \end{bmatrix} = \begin{bmatrix} \Sigma_{11}^R(\omega, \bar{i}) & -\Sigma_{12}^R(\omega, \bar{i}) \\ -\Sigma_{21}^R(\omega, \bar{i}) & \Sigma_{22}^R(\omega, \bar{i}) \end{bmatrix}. \quad (8)$$

We note that, although $G_{12,21}(\omega, y)$ are comparable to $G_{11,22}(\omega, y)$ in magnitude around the edges, they are strongly suppressed in the bulk. They become exactly zero at the center of the system if L_y is odd, as can be seen in the above identities.

B. DMFT + NRG calculations

We will now discuss the correlation effects in small size TIs from moderate to strong coupling within the inhomogeneous DMFT using the numerical renormalization group (NRG)^{56,57} as an impurity solver. The system size is fixed as $L_y = 10$. If nothing else is stated, we use a discretization parameter $\Lambda = 3.0$ and $N_K = 5000$ states are kept in the calculations. The effective impurity Anderson model for a single lattice site reads

$$\begin{aligned} H_{\text{IAM}}(y) &= H_c(y) + H_{\text{hyb}}(y) + H_{\text{imp}}(y), \\ H_c &= \sum_{ms, l'l'\sigma} a_{l'\sigma}^\dagger(ms) g_{ll'\sigma}(ms) a_{l\sigma}(ms), \\ H_{\text{hyb}} &= \sum_{ms, l'l'\sigma} \left[f_{l\sigma}^\dagger h_{ll'\sigma}(ms) a_{l'\sigma}(ms) \right. \\ &\quad \left. + a_{l'\sigma}^\dagger(ms) h_{l'l\sigma}^*(ms) f_{l\sigma} \right], \\ H_{\text{imp}} &= \sum_{l\sigma} E_{l\sigma}^f f_{l\sigma}^\dagger f_{l\sigma} + H_{\text{int}}[f_{l\sigma}^\dagger, f_{l\sigma}], \end{aligned}$$

where the parameters are determined self-consistently within the DMFT loop and depend on the y -index of

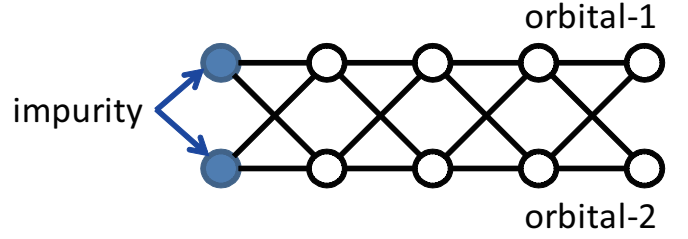


FIG. 9: (Color online) A schematic picture of the NRG chain Hamiltonian of the effective impurity Anderson model.

the lattice. Details for the derivation of the parameters are given in Appendix A 1 and A 2. The Hamiltonian can be rewritten as a linear chain as shown in Fig. 9. To examine the effects induced by strong correlations, the NRG is expected to be a very accurate impurity solver, especially near the Fermi energy.^{56,57} However, due to the SO interaction and the resulting inter-orbital hopping in the chain Hamiltonian, truncation effects can become large in these calculations. Therefore, the NRG must also be considered as an approximation even around the Fermi energy. (A discussion on truncation effects is given in Appendix A 3.) Furthermore, instead of using the usual logarithmic broadening of the delta-peaks in the Green's functions calculated by the NRG,⁵⁷ we use a Lorentzian broadening. The reason for this choice is, that the usual logarithmic broadening seems to be more fragile towards breaking of the symmetries discussed above. Using a Lorentzian broadening turned out to be much more stable. Nevertheless, NRG, being non-perturbative, can provide results for selfenergies and spectral functions, from which the ground state properties can be estimated. To our knowledge, the NRG has never been used for systems with inter-site inter-orbital hopping.

As discussed in the beginning of this section, the structures of the selfenergy can distinguish usual topological insulating states from possible edge Mott insulating states. Therefore, we first look at the ω -dependence of the selfenergy. In Fig. 10, $\Sigma(\omega, y)$ for $U = 8$ is shown as an example. A general feature is that the off-diagonal elements are much smaller than the diagonal elements. Furthermore, the selfenergy for any site y can be well approximated by $\Sigma(\omega, y) = [\Sigma(0, y) + (1 - z(y)^{-1})\omega - ib(y)\omega^2]$, where $z(y) = [1 - \partial\Sigma(y)/\partial\omega]_{\omega=0}^{-1}$. This behavior of $\Sigma_{11,22}$ is similar to those in correlated metals. Therefore, the result can be characterized as a renormalized gapped Fermi-liquid with renormalization factor $z(y)$ and quasi-particle broadening $\sim b(y)\omega^2$. There are no characteristic features in $\Sigma(\omega)$, such as isolated poles at $|\omega| < \Delta_{\text{TI}}$, which would drive the edge states into Mott insulating states. Moreover, the prefactors $b(y)$ are significantly smaller than those in metals, because the density of states around $\omega \simeq 0$ is suppressed by the bulk gap. This simple ω -dependence of $\Sigma(\omega)$ agrees with the previous DMFT+IPT calculations. DMFT+NRG confirms that this dependence actually holds for larger values of U than the band width W . The edge states always remain renor-

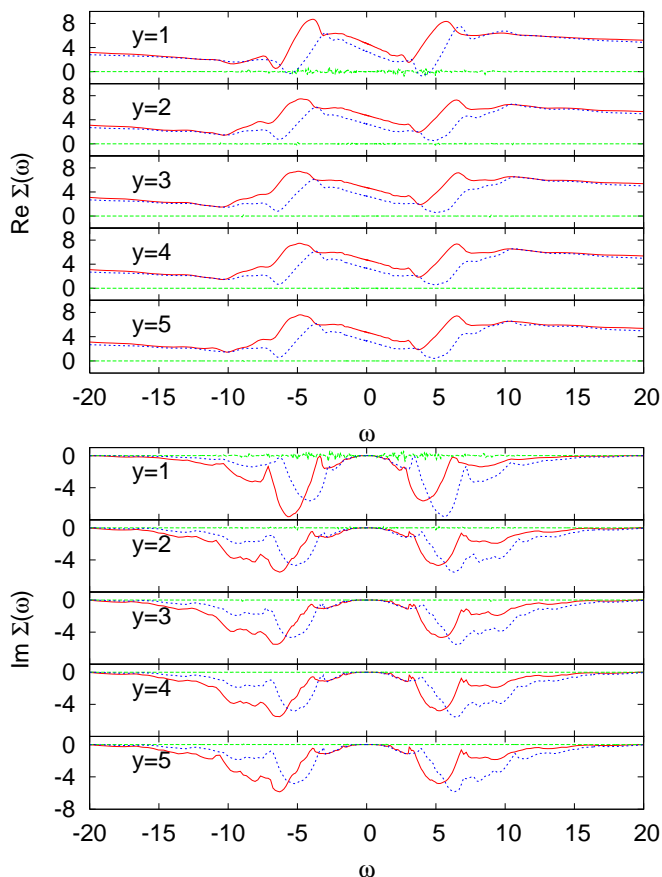


FIG. 10: (Color online) Selfenergy for $U = 8$ and $L_y = 10$. Red, green, blue curves are Σ_{11} , $\Sigma_{12,21}$ and Σ_{22} , respectively.

malized massive Dirac fermions as long as U is smaller than the critical value of the Mott transition U_c . The edge Mott insulating states are not found in our calculations. Possible inter-edge Umklapp scattering does not seem to have significant effects on the edge states, although its coupling constant $g_{h,f}$ might be large compared to the gap width $\Delta_{f,\text{TI}}$ when $U \gg \Delta_{f,\text{TI}}$. We note that all correlation effects can be characterized by a single quantity U/W , and concerning the Mott insulator transition, $U \sim \Delta_{\text{TI}}$ does not introduce a new characteristic energy scale, although Δ_{TI} can seemingly characterize the effective band width of the edge states.

Although we cannot find the edge Mott insulating states in the present calculations, there is another possibility for Mott insulating states to appear. In inhomogeneous strongly correlated systems, such as optical lattices with harmonic potentials,⁵⁰ Mott insulating behaviors in some domains of the systems have been found at finite temperatures. For these states, the site dependence of local correlations is most important.

In the following, we will discuss the spatial dependence of correlation effects by looking at the renormalization factors $z(y)$. In Fig. 11, we compare $z(y)$ for several values of the interaction strength U . While for weak interactions, the y -dependence of $z(y)$ is moderate, for

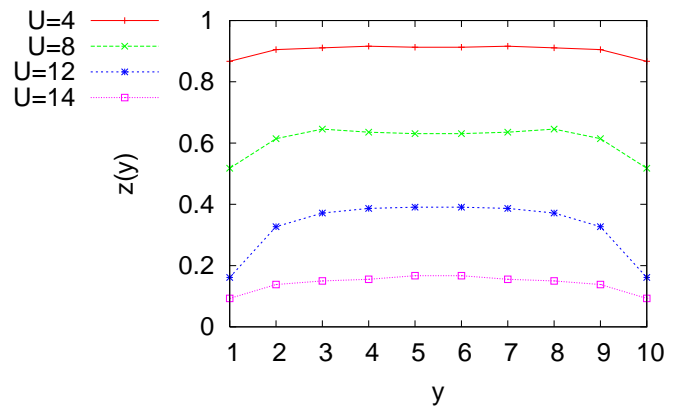


FIG. 11: (Color online) The renormalization factor $z(y)$ for several values of U for $L_y = 10$.

strong interactions, e.g. $U = 12$ and $U = 14$, which are close to the critical value for the Mott transition, $z(y)$ is largely suppressed, especially at the edge sites. That can be understood by recalling that the coordination number at the edge sites is smaller than in the bulk, which restricts the electron motions at the edges. Strong correlation effects at boundaries due to the reduction of the coordination number have been discussed in the literature for various systems, such as metallic surfaces,^{44,45} heterostructures,^{46–49} optical lattices,^{50–53} and spin systems.⁵⁸ Even though the electrons are largely renormalized especially around the edges, $z(y)$ is nonzero for all the sites and the bulk gap due to the SO interaction remains finite. This state can be characterized as a renormalized TI, and therefore can be adiabatically connected to the non-interacting TI without closing the gap. In this sense, the system remains topologically unchanged for all interaction strengths $U < U_c$, where U_c is the critical interaction strength for the Mott transition.

The orbital averaged local density of states $-(1/2\pi)\text{Im}(G_{11} + G_{22})$ for small ω directly shows the renormalization effects as seen in Fig. 12. Small dips inside the bulk gap correspond to the finite size gap, and finite values for $|\omega| < \Delta_{\text{TI}}$ are due to the massive Dirac edge states. As has been discussed in Sec. II B, both Δ_{TI} and Δ_f are renormalized in a similar way.

For larger values of U , $U > 14$, the renormalization factors become zero $z(y) = 0$ for all y , signaling Mott insulating states for all sites. Our results are qualitatively equivalent to the results for the single band Hubbard model where both edges and bulk are metallic without interactions. Although $z(y)$ decreases especially around the edge sites, as has also been found in the previous studies^{43–49}, $z(y)$ vanishes for all y at the same time at zero temperature, and a nearly homogeneous Mott insulating state is stabilized. This can be explained by quantum tunneling of electrons from the bulk to the edges. If the bulk stays metallic, then, the edges are imposed to be metallic even though z at the edges is strongly suppressed.

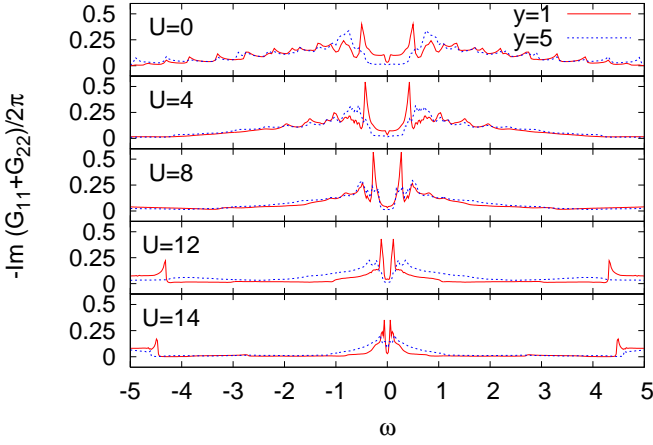


FIG. 12: (Color online) The local density of states at $y = 1$ (red curve) and $y = 5$ (blue curve) for several values of $U < U_c$.

In the TIs, on the other hand, the bulk is gapful, and therefore, one could expect that the quantum tunneling of electrons is diminished, which possibly leads to inhomogeneous solutions where only the edges are gapped with a Mott gap Δ_{MI} . Such solutions could be interpreted as heterostructures of Mott insulators and TIs. Nevertheless, the Mott insulating sites near the edges can reduce the effective system size of the TI, leading to an enhanced finite size gap.

However, as mentioned above, inhomogeneous Mott insulating states are not obtained in our zero temperature calculations. The absence of such inhomogeneous solutions can already be understood within the linearized DMFT. As was shown in Figs. 4 and 10, the local self-energy can be approximated as $\Sigma_{11,22}(\omega, y) = \Sigma_{11,22}(0, y) + (1 - z(y)^{-1})\omega + \mathcal{O}(\omega^2)$ for small ω , and $\Sigma_{12,21}$ is much smaller than $\Sigma_{11,22}$ in magnitude and can be neglected. In this approximation, $\Sigma(\omega)$ has the same structure as a simple two orbital metallic system, and the discussions in the previous studies^{43–45,48,49} can be easily applied to the system. Within the linearized DMFT, inhomogeneous solutions such as $z(y = 1, L_y) = 0$ and $z(1 < y < L_y) \neq 0$ are not stable provided that $\Sigma_{12,21}$ is negligible. Because the bulk gap is generated by the inter-site inter-orbital hopping, the gap generating mechanism extends to the edge by electron motions, making the whole system topological insulating. In other words, the system is never cut by $z = 0$ at specific sites when the interaction strength is increased. This argument is based upon the linearized DMFT equations and is a direct consequence of the simple structure of the local self-energy $\Sigma_{ll'}(\omega, y) \simeq [\Sigma_{ll'}(0, y) + (1 - z(y)^{-1})\omega]\delta_{ll'}$ which can be checked in the DMFT+NRG and DMFT+IPT calculations. We also note that, even if spatial correlations are taken into account within cluster extensions of the DMFT, Mott transitions for large size systems are expected to be homogeneous.⁷²

However, especially at the edge sites, the Fermi-liquid

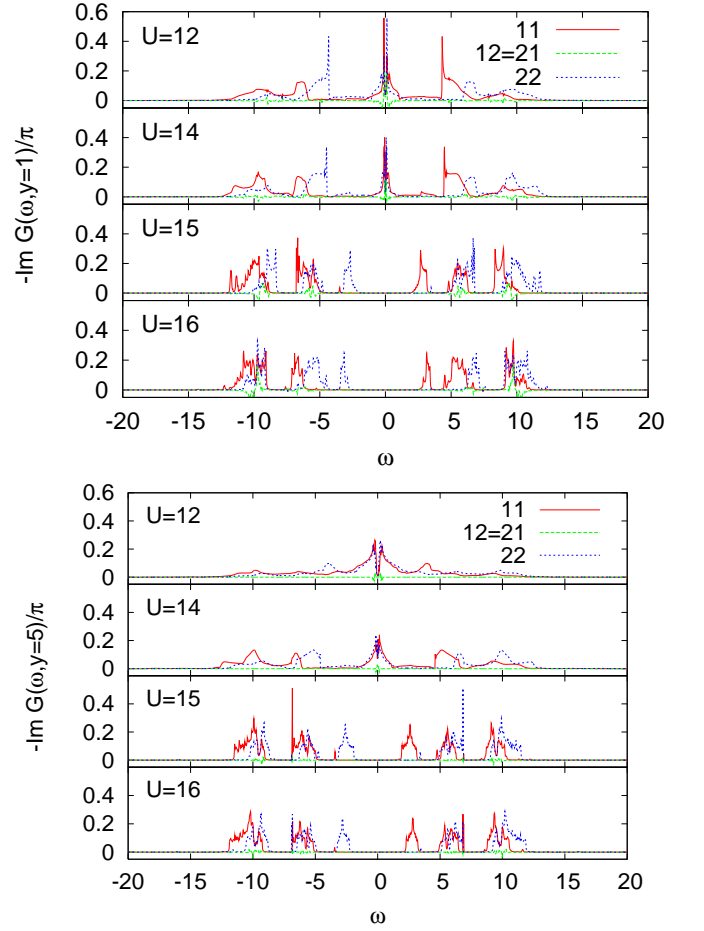


FIG. 13: (Color online) The imaginary parts of the local Green's functions for several values of U at $y = 1$ (upper panel) and $y = 5$ (lower panel) when $L_y = 10$. Red, green, blue curves are $G_{11}, G_{12,21}$ and G_{22} , respectively.

behavior in our system would be fragile against temperatures, and Mott insulating domains could be seen at finite temperatures as it was discussed in the literature.^{49,50} One can expect that there are temperature ranges where the peak structures around $\omega \sim 0$ in the local density of states at the edge sites disappear, while they survive in the bulk. In such a case, Mott insulating domains could grow from the edges to the bulk as U is increased. Finite temperature studies will be discussed in the future.

Finally, we briefly discuss the gap structures in the imaginary part of the local Green's functions which correspond to the local density of states. Figure 13 shows $\text{Im}G$ for several different interaction strengths U . With increasing U for $U < U_c$, the structures around the Fermi energy become more and more renormalized, and finally for $U > U_c$ a Mott gap with $\Delta_{\text{MI}} \sim U$ opens. Here, we note that the Mott transition as a topological phase transition is qualitatively different from transitions in which parameters in the non-interacting part of the Hamiltonian are changed. For example, if the parameter M_0 is changed (for $U = 0$), a transition from a TI to a

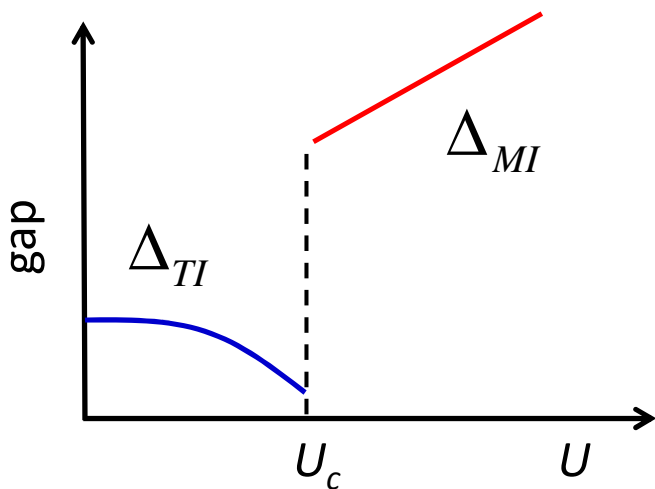


FIG. 14: (Color online) A schematic picture of the U -dependence of Δ_{TI} and Δ_{MI} . At finite temperatures or if spatial correlations are taken into account, Δ_{TI} would not close and the transition would be discontinuous.

trivial band insulator will occur. However, the gap in both phases is well defined in momentum-space. The gap width in each phase is changing continuously near the topological phase transition. At the Mott transition, however, the well-defined gap in momentum-space Δ_{TI} for the TI phase is replaced by the Mott gap Δ_{MI} which arises due to a gap in the atomic electron configurations in real space. Although the Mott transition would be continuous in the present calculations with the DMFT at zero temperature, at finite temperatures or if spatial correlations are taken into account, the transition can be expected to be discontinuous.^{25,42,73} The schematic behavior of the gap is shown in Fig. 14.

Finally, let us make some comments on $\Sigma_{12,21}$. As mentioned in the previous section, the local selfenergy satisfies $\Sigma_{12,21}(\omega, y) = -\Sigma_{12,21}(\omega, y)^*$, and especially, $\text{Re}\Sigma_{12,21}(\omega = 0, y) = 0$ for all y sites. However, $\text{Im}\Sigma_{12,21}(\omega = 0, y)$ does not necessarily have to vanish due to symmetry arguments. Although our calculated $\Sigma_{12,21}$ is much smaller than $\Sigma_{11,22}$ and could be safely neglected, we have small but finite values of $\Sigma_{12,21}(\omega = 0, y)$ near the edge sites. This might be related to the inter-edge Umklapp scattering. However, since $\Sigma_{12,21}(\omega)$ shows complicated ω -dependence within the NRG calculations, it is difficult to evaluate $\Sigma_{12,21}(\omega = 0)$ with sufficient accuracy.

IV. SUMMARY AND DISCUSSION

In this article we have discussed correlation effects in two dimensional topological insulators. In the first part, we investigated finite size effects in relatively large systems. The effective theory for those edge states is given by one-dimensional spin-1/2 fermions including inter-edge correlated forward scattering.

The Tomonaga-Luttinger parameters are $K_s \geq 1$ for the spin sector and $K_c \leq 1$ for the charge sector. They include the renormalization factor defined in the whole two dimensional system and might not be so much away from unity. The analysis of the scaling dimensions of the perturbations revealed that the tunneling between two edges is the most relevant perturbation around the non-interacting point when the Fermi wavenumber of the edge states is $k_F \sim 0$. We evaluated the gap size induced by the tunneling for each sector which might be observed in experiments.

For small systems, the edge states are massive Dirac fermions and there are no massless single particle excitations. We discussed the correlation effects by using the inhomogeneous DMFT with the IPT in the ribbon geometry. We confirmed that the naive expectation based on the Fermi-liquid picture of the correlated TIs, that the amplitude of the finite size gap is simply renormalized by the averaged renormalization factor, and the localization length of the edge states is not affected by the interaction, actually holds for weak interactions.

Finally, we discussed the Mott transition using the inhomogeneous DMFT+NRG. The ω -dependence of the selfenergy is qualitatively similar to that in the metallic systems. We could not see characteristic features in the selfenergy which signal the edge Mott insulating states, although inter-edge Umklapp scattering is taken into account within DMFT. We showed that correlation effects are significantly stronger near the edge sites due to the reduction of the coordination number. Since the edge states are localized around the edges, the relatively strong correlations largely affect them especially near the Mott transition. As the interaction is tuned, we found a trivial Mott transition from the topological insulating state to a nearly homogeneous Mott insulating state. The numerical results can also be understood within the linearized DMFT as a result of the quantum tunneling of the electrons as has been discussed for systems without bulk gaps. The transition to a Mott insulator is characterized as a topological phase transition, and the character of the gap in each phase is totally different and the gap closing is not required at the transition in general.

In the present DMFT calculations, we have focused on the paramagnetic phase and neglected instabilities to magnetically ordered phases.²⁵ However, in addition to homogeneous magnetic states, magnetic moments only near the edge sites might be possible.^{74,75} We also assumed that all parameters in the Hamiltonian are uniform, although there can be changes especially near the edge sites in experimental situations. These issues are future problems.

Acknowledgment

We thank T. Yoshida for valuable discussions. Numerical calculations were partially performed at the Yukawa Institute Computer Facility. This work is

partly supported by the Grant-in-Aids for Scientific Research from MEXT of Japan (Grant No.19052003, Grant No.20102008, Grant No.20740194, Grant No.21102510, Grant No.21540359, Grant No.23540406, and Grant No.23840009), and the Grant-in-Aid for the Global COE Program "The Next Generation of Physics, Spun from Universality and Emergence" and "Nanoscience and Quantum Physics". RP thanks the Japan Society for the Promotion of Science (JSPS) and the Alexander von Humboldt-Foundation. NK is partly supported by JSPS through the "Funding Program for World-Leading Innovative R&D on Science and Technology (FIRST Program)".

Appendix A: Details of NRG

In this Appendix, we show details of the NRG formalism. DMFT + NRG calculations with off-diagonal selfenergy have been performed in the context of superconductivity,^{70,71} and our treatment is an extension of the previous works. We also discuss details of the numerical calculations.

1. Effective Impurity Anderson model

The impurity model arising from the DMFT self-consistency reads

$$\begin{aligned} H_{\text{IAM}}(y) &= H_c(y) + H_{\text{hyb}}(y) + H_{\text{imp}}(y), \\ H_c &= \sum_{ms, ll'\sigma} a_{l\sigma}^\dagger(ms) g_{ll'\sigma}(ms) a_{l'\sigma}(ms), \\ H_{\text{hyb}} &= \sum_{ms, ll'\sigma} \left[f_{l\sigma}^\dagger h_{ll'\sigma}(ms) a_{l'\sigma}(ms) \right. \\ &\quad \left. + a_{l'\sigma}^\dagger(ms) h_{ll'\sigma}^*(ms) f_{l\sigma} \right], \\ H_{\text{imp}} &= \sum_{l\sigma} E_{l\sigma}^f f_{l\sigma}^\dagger f_{l\sigma} + H_{\text{int}}[f_{l\sigma}^\dagger, f_{l\sigma}] \end{aligned}$$

where

$$E^f = (M_0 - \mu, -M_0 - \mu).$$

The impurity is represented by the operators $f_{l\sigma}$, where l is the orbital- and σ the spin index. The conduction electrons are given by the operators $a_{l\sigma}(ms)$, where ms corresponds to an discretization interval $(m+)$, $(m-)$ as defined below. Therefore, in this context $g_{ll'}$ corresponds to the kinetic energy, while $h_{ll'}$ corresponds to the hybridization between impurity and conduction electrons. Note that all the parameters in H_{IAM} depend on the site index y , which is suppressed for clarity of the notation. From now on, we will neglect the spin indices, because the lattice Hamiltonian is diagonal in spin space. The energy is discretized into intervals

$$\begin{aligned} I_{m+} &= (x_{m+1}, x_m] \\ I_{m-} &= (-x_m, -x_{m+1}], \end{aligned}$$

with $x_m = x_0 \Lambda^{-m}$ ($m \in \mathbb{N}$).

We consider the particle-hole symmetric case and assume that $g_{ll'}(ms) \in \mathbb{R}$ and can be written as

$$g(ms) := \begin{bmatrix} \xi(ms) & \mathcal{L}(ms) \\ \mathcal{L}(ms) & -\xi(ms) \end{bmatrix}. \quad (\text{A1})$$

This assumption is legitimate, because our lattice Hamiltonian is defined only by real values when using open boundary conditions for the y -direction. The hybridization h is parametrized as

$$h(ms) = \begin{bmatrix} a(ms) & b(ms) \\ b'(ms) & c(ms) \end{bmatrix},$$

where a, b, b' and c are also assumed to be real.

The kinetic energy term g is diagonalized by the following orthogonal matrices,

$$\begin{aligned} U(ms) &= \begin{bmatrix} u(ms) & -v(ms) \\ v(ms) & u(ms) \end{bmatrix}, \\ u^2(ms) &= \frac{1}{2} \left(1 + \frac{\xi(ms)}{E(ms)} \right), \\ v^2(ms) &= \frac{1}{2} \left(1 - \frac{\xi(ms)}{E(ms)} \right), \\ E(ms) &= \sqrt{\xi^2(ms) + \mathcal{L}^2(ms)}. \end{aligned}$$

$E(ms)$ can finally be identified (for both $s = \pm$) as

$$E(ms) = |x_m + x_{m+1}|/2,$$

corresponding to the discretized intervals. The kinetic energy and the hybridization are transformed as

$$\begin{aligned} \tilde{g}(ms) &= U^\dagger g(ms) U \\ &= \begin{bmatrix} E(ms) & 0 \\ 0 & -E(ms) \end{bmatrix}, \\ \tilde{h}(ms) &= h(ms) U(ms) \\ &= \begin{bmatrix} au + bv & -av + bu \\ b'u + cv & -b'v + cu \end{bmatrix} \\ &\equiv \begin{bmatrix} A & B \\ B' & C \end{bmatrix}. \end{aligned}$$

Then, in this new basis \tilde{a} , the impurity Anderson Hamiltonian is written as

$$\begin{aligned} H_c &= \sum_{ms, \alpha} \tilde{a}_\alpha^\dagger(ms) E_\alpha(ms) \tilde{a}_\alpha(ms), \\ H_{\text{hyb}} &= \sum_{ms, l, \alpha} [f_l^\dagger \tilde{h}_{l\alpha}(ms) \tilde{a}_\alpha(ms) + \tilde{a}_\alpha^\dagger(ms) \tilde{h}_{l\alpha}(ms) f_l], \\ \tilde{a}_\alpha(ms) &= \sum_l U_{\alpha l}^\dagger(ms) a_l(ms), \end{aligned}$$

where $E_\alpha(ms) = (E(ms), -E(ms))$.

The retarded non-interacting Green's function of the impurity Anderson model can be written as,

$$\mathcal{G}^{-1}(\omega + i0) = \omega - E^f - K(\omega + i0),$$

where the hybridization K is given as,

$$\begin{aligned} K_{ll'}(\omega) &= \sum_{ms} (h(ms)[\omega - g(ms)]^{-1} h^\dagger(ms))_{ll'} \\ &= \sum_{ms} ((hU)[\omega - U^\dagger gU]^{-1} (U^\dagger h^\dagger))_{ll'} \\ &= \sum_{ms} \sum_{\alpha} \frac{\tilde{h}_{l\alpha} \tilde{h}_{l'\alpha}}{\omega - E_{\alpha}}. \end{aligned}$$

Using the identity $1 = \int d\varepsilon \delta(\varepsilon - E_{\alpha}(ms))$ for each α , we obtain

$$\begin{aligned} K_{ll'}(\omega) &= \int d\varepsilon \frac{\Delta_{ll'}(\varepsilon)}{\omega - \varepsilon + i0}, \\ \Delta_{ll'}(\varepsilon) &= \sum_{ms, \alpha} \tilde{h}_{l\alpha}(ms) \tilde{h}_{l'\alpha}(ms) \delta(\varepsilon - E_{\alpha}(ms)). \end{aligned}$$

We note that due to the Kramers-Kronig relation,

$$\Delta(\omega) = -\frac{1}{\pi} \text{Im}K(\omega)$$

is satisfied.

Next, for each interval I_{ms} , we define

$$\Delta(ms) = \int_{I_{ms}} d\omega \Delta(\omega).$$

Thus, for the integral region I_{m_0+} which includes only a single value $E(ms) \in \{E(n\sigma)\}_{n\sigma}$, the following equations hold

$$\Delta_{ll'}(m+) = \sum_s \tilde{h}_{l1}(ms) \tilde{h}_{l'1}(ms), \quad (\text{A2})$$

and for I_{m_0-} ,

$$\Delta_{ll'}(m-) = \sum_s \tilde{h}_{l2}(ms) \tilde{h}_{l'2}(ms). \quad (\text{A3})$$

The number of obtained equations for \tilde{h} given by Eqs. (A2) and (A3) is six. $\Delta_{11}(m\pm), \Delta_{22}(m\pm), \Delta_{12}(m\pm)$ are involved and Δ_{21} gives the same equations as Δ_{12} . However, the number of independent $\tilde{h}_{l\alpha}$ is eight and two extra conditions are needed for $\tilde{h}_{l\alpha}$ to be determined. One possibility is that extra conditions are imposed so that \tilde{h} is connected smoothly to the trivial situation if we turn off the SO interaction, which is legitimate because $|h_{11,22}| > |h_{12,21}|$ is expected in general physical situations.

Taking the limit $\mathcal{L} \rightarrow +0$ for the entries of the conduction electrons of the original untransformed impurity model (Eq A1) and because $\xi(m+) > 0$ and $\xi(m-) < 0$ can be assumed, the limiting behaviors of u, v should be

$$\begin{aligned} u(m+) &\rightarrow 1, & v(m+) &\rightarrow 0, \\ u(m-) &\rightarrow 0, & v(m-) &\rightarrow 1, \end{aligned}$$

and

$$\begin{aligned} \tilde{h}(m+) &\rightarrow \begin{bmatrix} a(m+) & b(m+) \\ b'(m+) & c(m+) \end{bmatrix}, \\ \tilde{h}(m-) &\rightarrow \begin{bmatrix} b(m-) & -a(m-) \\ c(m-) & -b'(m-) \end{bmatrix}. \end{aligned}$$

Therefore, a possible additional condition which keeps the symmetry of \tilde{h} is, $A(m-) = -B'(m+)$ and $C(m-) = +B(m+)$. These conditions are linear in \tilde{h} . In the limit $\mathcal{L} \rightarrow 0$, the first equation corresponds to $b_- = -b'_+$, and the second one to $-b'_- = b_+$. Here, we have used shortened expressions $X_s = Y_{s'}$ for $X(ms) = Y(ms')$. Then, the equations for \tilde{h} are,

$$\begin{aligned} \Delta_{11+} &= A_+^2 + A_-^2, \\ \Delta_{22+} &= B_+'^2 + B_-'^2 = A_-^2 + B_-'^2, \\ \Delta_{12+} &= A_+ B_+' + A_- B_- = A_- (-A_+ + B_-'), \\ \Delta_{11-} &= B_+^2 + B_-^2 = C_-^2 + B_-^2, \\ \Delta_{22-} &= C_+^2 + C_-^2, \\ \Delta_{12-} &= C_+ B_+ + C_- B_- = C_- (C_+ + B_-) \end{aligned}$$

In this set of equations the upper three and lower three equations are decoupled. Because these equations are non-linear and have several possible solutions, the solution which can be smoothly connected to the limit $\mathcal{L} \rightarrow +0$ and $b, b' \rightarrow 0$ should be carefully chosen. The results are,

$$\begin{aligned} \delta_s &\equiv -\frac{(\Delta_{12s})^2}{(\Delta_{11s} - \Delta_{22s})^2 + 4\Delta_{12s}^2} \left[(\Delta_{11s} + \Delta_{22s}) \right. \\ &\quad \left. - 2\sqrt{\Delta_{11s}\Delta_{22s} - \Delta_{12s}^2} \right], \\ A_+ &= \sqrt{\Delta_{11+} + \delta_+}, \\ A_- &= -\frac{\Delta_{12+}}{\sqrt{\Delta_{11+} + \delta_+} + \sqrt{\Delta_{22+} + \delta_+}}, \\ B_+' &= -A_-, \\ B_-' &= -\sqrt{\Delta_{22+} + \delta_+}, \\ C_+ &= -\sqrt{\Delta_{22-} + \delta_-}, \\ C_- &= -\frac{\Delta_{12-}}{\sqrt{\Delta_{11-} + \delta_-} + \sqrt{\Delta_{22-} + \delta_-}}, \\ B_+ &= C_-, \\ B_- &= -\sqrt{\Delta_{11-} + \delta_-}. \end{aligned}$$

Note that for the above solution of δ_s ,

$$\lim_{\Delta_{22s} \rightarrow \Delta_{11s}} \lim_{\Delta_{12s} \rightarrow 0} \delta_s = \lim_{\Delta_{12s} \rightarrow 0} \lim_{\Delta_{22s} \rightarrow \Delta_{11s}} \delta_s = 0$$

is satisfied and δ_s is smoothly connected to the case without the SO interaction. Because we focus on the particle-hole symmetric case with $\Delta_{11\pm} = \Delta_{22\mp}, \Delta_{12+} = \Delta_{12-}$, some relations can be derived from the above expressions of $A \sim C$: $\delta_+ = \delta_-, A_+ = -C_+, B_+' = -B_+, A_- = C_-$

and $B'_- = B_-$. The resulting \tilde{h} has the form of

$$\begin{aligned}\tilde{h}(m+) &= \begin{bmatrix} A(m+) & B(m+) \\ -B(m+) & -A(m+) \end{bmatrix} \\ &\rightarrow \begin{bmatrix} \sqrt{\Delta_{11}(m+)} & 0 \\ 0 & -\sqrt{\Delta_{11}(m+)} \end{bmatrix}, \\ \tilde{h}(m-) &= \begin{bmatrix} A(m-) & B(m-) \\ B(m-) & A(m-) \end{bmatrix} \\ &\rightarrow \begin{bmatrix} 0 & -\sqrt{\Delta_{11}(m-)} \\ -\sqrt{\Delta_{11}(m-)} & 0 \end{bmatrix},\end{aligned}$$

where ' \rightarrow ' means the limit $\mathcal{L} \rightarrow 0$ and $b, b' \rightarrow 0$. Correspondingly, $h(ms) = \tilde{h}(ms)U^\dagger(ms) \rightarrow \text{diag}(\sqrt{\Delta_{11}(ms)}, -\sqrt{\Delta_{11}(ms)})$.

We note that a condition is required for A, B, B' and C to be real quantities:

$$-\max\{\Delta_{11s}, \Delta_{22s}\} \leq \delta_s \leq 0. \quad (\text{A4})$$

Another condition is needed for δ_\pm to be real:

$$\Delta_{11s}\Delta_{22s} - \Delta_{12s}^2 \geq 0. \quad (\text{A5})$$

These two conditions are essentially equivalent. The above derivation is based on the assumption that \tilde{h} should be connected smoothly to the one without the SO interaction, $\mathcal{L}, b, b' \rightarrow 0$. If one assumes other smooth connections, such as a connection to $\xi \rightarrow 0$, different expressions for $A \sim C$ would be obtained.

2. Chain Hamiltonian

In the next step we transform H_{IAM} into a chain Hamiltonian. We want to transform the impurity Anderson model to

$$\begin{aligned}H_c &= \sum_{n\nu\nu'\sigma} \varepsilon_{n\nu\nu'} f_{n\nu\sigma}^\dagger f_{n\nu'\sigma} \\ &+ \sum_{n\nu\nu'\sigma} t_{n\nu\nu'} [f_{n\nu\sigma}^\dagger f_{n+1\nu'\sigma} + f_{n+1\nu'\sigma}^\dagger f_{n\nu\sigma}], \\ H_{hyb} &= \sum_{\nu\nu'\sigma} v_{\nu\nu'} [f_{-1\nu\sigma}^\dagger f_{0\nu'\sigma} + f_{0\nu'\sigma}^\dagger f_{-1\nu\sigma}], \\ H_{imp} &= \sum_{\nu\sigma} E_\nu^f f_{-1\nu\sigma}^\dagger f_{-1\nu\sigma} + H_{int}[f_{-1\nu\sigma}^\dagger, f_{-1\nu\sigma}].\end{aligned}$$

Here, $f_{-1\nu}$ corresponds to the former f_α ,

$$f_{-1\nu} = \sum_\alpha \delta_{\alpha\nu} f_\alpha.$$

This chain Hamiltonian is schematically shown in Fig. 9 of the main text. Because the impurity part H_{imp} is not transformed from its original expression and H_c again includes the inter-chain hopping, we understand that the index ν in the basis $\{f_{n\nu\sigma}\}$ characterizes the orbitals $l = 1, 2$. As far as we know, impurity Anderson

models with inter-chain hopping have never been studied by using NRG. The inter-chain hopping in the present model arises from the inter-orbital hopping, and it makes numerical calculations hard.

Let us assume that this transformation is given by an orthogonal matrix $u = (u_{nm}^{\nu\alpha})$,

$$f_{n\nu} = \sum_{ms\alpha} u_{nm}^{\nu\alpha} \tilde{a}_\alpha(ms),$$

$$\tilde{a}_\alpha(ms) = \sum_{n\nu} u_{nm}^{\nu\alpha} f_{n\nu},$$

$$\sum_{ms\alpha} u_{nm}^{\nu\alpha} u_{n'm'}^{\nu'\alpha} = \delta_{nn'} \delta_{\nu\nu'},$$

$$\sum_{n\nu} u_{nm}^{\nu\alpha} u_{n'm'}^{\nu'\alpha} = \delta_{mm'} \delta_{ss'} \delta_{\alpha\alpha'}.$$

Then, the hybridization term would be,

$$\begin{aligned}H_{hyb} &= \sum_{msl\alpha} [f_l^\dagger \tilde{h}_{l\alpha}(ms) \tilde{a}_\alpha(ms) + \text{h.c.}] \\ &= \sum_{n\nu\nu'} f_{-1\nu}^\dagger \left[\sum_{ms\alpha} \tilde{h}_{\nu\alpha}(ms) u_{nm}^{\nu\alpha} \right] f_{n\nu'} + (\text{h.c.}).\end{aligned}$$

We define a vector $(\tilde{u}_0^\nu)_{ms}^\alpha = \tilde{u}_{0ms}^{\nu\alpha}$ and an inner product as

$$\begin{aligned}\tilde{u}_{0ms}^{\nu\alpha} &= \tilde{h}_{\nu\alpha}(ms), \\ \langle u_n^\nu, u_{n'}^{\nu'} \rangle &\equiv \sum_{ms\alpha} u_{nm}^{\nu\alpha} u_{n'm'}^{\nu'\alpha},\end{aligned}$$

and normalize $\tilde{u}_{0ms}^{\nu\alpha}$ as $\bar{u}_{0ms}^{\nu\alpha} = \tilde{u}_{0ms}^{\nu\alpha} / \sqrt{|\langle \tilde{u}_0^\nu, \tilde{u}_0^\nu \rangle|}$. We, then, orthogonalize $\{\bar{u}_0^1, \bar{u}_0^2\}$ keeping their symmetry to obtain $\{u_0^1, u_0^2\}$. To fulfill symmetry requirements, the trigonalization must be performed always by including two vectors. Therefore, we assume that orthogonalization can be performed by

$$\begin{aligned}\bar{u}_0^{1new} &= \bar{u}_0^1 + c \langle \bar{u}_0^1, \bar{u}_0^2 \rangle \bar{u}_0^2, \\ \bar{u}_0^{2new} &= \bar{u}_0^2 + c \langle \bar{u}_0^1, \bar{u}_0^2 \rangle \bar{u}_0^1\end{aligned}$$

with one coefficient c . Then, $\langle \bar{u}_0^{1new}, \bar{u}_0^{2new} \rangle = \langle \bar{u}_0^1, \bar{u}_0^2 \rangle [1 + 2c + c^2 \langle \bar{u}_0^1, \bar{u}_0^2 \rangle]$. If $c = -0.5$, $\langle \bar{u}_0^{1new}, \bar{u}_0^{2new} \rangle = 0.25 \times \langle \bar{u}_0^1, \bar{u}_0^2 \rangle^2$. Because \bar{u}_0^1 and \bar{u}_0^2 have been normalized, $|\langle \bar{u}_0^1, \bar{u}_0^2 \rangle| < 1$ is satisfied. Repeating this procedure leads to orthogonalized unit vectors $\{u_0^1, u_0^2\}$. The hopping from site -1 to site 0 is calculated from $\tilde{u}_{0ms}^{\nu\alpha} = \tilde{h}_{\nu\alpha}(ms)$ as

$$v_{\nu\nu'} = \langle \tilde{u}_0^\nu, \tilde{u}_0^{\nu'} \rangle.$$

Next, let us move to the kinetic term.

$$\begin{aligned}H_c &= \sum_{ms\alpha} E_\alpha(ms) \tilde{a}_\alpha^\dagger(ms) \tilde{a}_\alpha(ms) \\ &= \sum_{n\nu} \sum_{n'\nu'} \left[\sum_{ms\alpha} E_\alpha(ms) u_{nm}^{\nu\alpha} u_{n'm'}^{\nu'\alpha} \right] f_{n\nu}^\dagger f_{n'\nu'}.\end{aligned}$$

This claims that

$$\sum_{ms\alpha} E_\alpha(ms) u_{nms}^{\nu\alpha} u_{n'm's}^{\nu'\alpha} = \varepsilon_{n\nu\nu'} \delta_{nn'} + t_{n\nu\nu'} [\delta_{n',n+1} + \delta_{n,n'+1}]$$

should hold.

If $u_j^{\nu'}$, $j = 0, \dots, n$ are obtained, we calculate $\varepsilon_{n\nu\nu'}$ from

$$\varepsilon_{n\nu\nu'} = \sum_{ms\alpha} E_\alpha(ms) u_{nms}^{\nu\alpha} u_{nms}^{\nu'\alpha}.$$

Then, we define

$$\tilde{u}_{n+1ms}^{\nu\alpha} = \sum_{\nu', m's\alpha} \left[(E_\alpha(ms) \delta_{\nu\nu'} - \varepsilon_{n\nu\nu'}) u_{nms}^{\nu'\alpha} - t_{n-1\nu\nu'} u_{n-1ms}^{\nu'\alpha} \right],$$

and normalize each of $\tilde{u}_{n+1}^{1,2}$ to obtain normalized vectors $\bar{u}_{n+1}^{1,2}$. Using $\bar{u}_{n+1}^{1,2}$ as initial vectors, we perform the orthogonalization introduced above. and obtain orthogonal vectors $\{u_{n+1}^1, u_{n+1}^2\}$. Usual Schmidt orthogonalization should also be imposed so that $\langle u_{n+1}^{\nu'}, u_j^{\nu'} \rangle = 0$ for $j = 0, \dots, n$ are satisfied. Then, we evaluate t_n as

$$t_{n\nu\nu'} = \sum_{ms\alpha} E_\alpha(ms) u_{nms}^{\nu\alpha} u_{n+1ms}^{\nu'\alpha}.$$

All the parameters in the above decrease exponentially, and the input Δ is well reproduced from the chain Hamiltonian derived in this way.

We note that, although our chain impurity Anderson model is rather complicated, it is smoothly connected to the one without the inter-orbital hopping which is nothing but two decoupled single-orbital impurity Anderson models when there are no inter-orbital interactions at the impurity site. The ground state of our impurity Anderson model is simply the Kondo screened state or the decoupled state depending on the structure of the hybridization Δ .

3. Discretization, Truncation and Broadening

As already mentioned in the main text, the NRG is not able to gain its usual accuracy around the Fermi energy due to the spin-orbit interaction which creates an hybridization between the two orbitals. For the most of our shown results we used a discretization $\Lambda = 3.0$ and a truncation of $N_K = 5000$ states. Although $N_K = 5000$ may sound a large number of kept states, one should compare this number to that for a single impurity Anderson model (SIAM) for which similar accuracy with $N_{SIAM} = \sqrt{5000} \approx 70$ states would be obtained. Reducing the discretization parameter Λ to the often used value of $\Lambda = 2.0$ results in a breaking of the symmetries discussed above, e.g. ($G_{12}(\omega) \neq G_{21}(\omega)$) which are

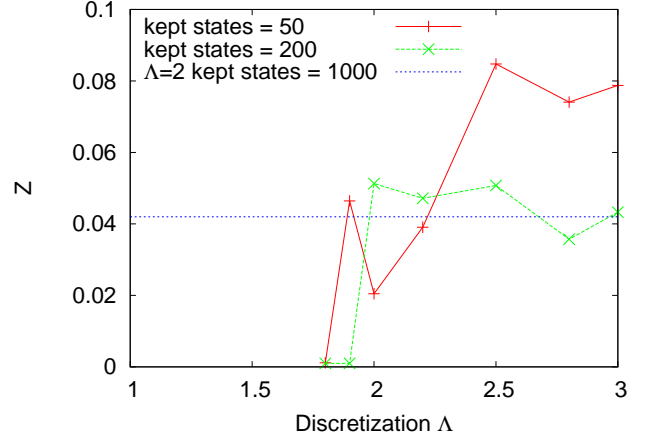


FIG. 15: (Color online) Truncation and discretization effects for the metal insulator transition in the ordinary one-orbital Hubbard model⁷⁶. We show the renormalization z for $U = 1.4W \approx 0.94U_c$. The lines are meant as guide to the eye. The blue line is the reference value calculated for $\Lambda = 2$, $N_K = 1000$ (independent of the discretization parameter).

supposed to be satisfied. To reduce the truncation effects and restore the symmetries we had to use a discretization parameter $\Lambda = 3.0$.

Therefore we briefly want to discuss the effects of discretization and truncations for the well studied metal insulator transition in the one-orbital Hubbard model at half filling.⁷⁶ In Fig. 15 we show the z -values $z = [1 - \partial\Sigma/\partial\omega]_{\omega=0}^{-1}$ for different truncations and discretization parameters Λ for an interaction strength $U = 1.4W \approx 0.94U_c$ close to the Mott transition at U_c . Large discretization parameters Λ lead to faster decreasing hopping parameters along the Wilson chain, reducing the effects of truncated high-energy states on the kept low-energy states, thus restoring the fundamental working principle of NRG. On the other hand, a large discretization parameter reduces the available number of states, and calculation results go away from those for the continuum limit $\Lambda \rightarrow 1$.

In the usual NRG iteration scheme, the renormalization procedure starts at high energies (large frequencies in the spectral functions) and iterates down to the Fermi energy (zero frequency in the spectral functions). Thus, using small discretization parameter Λ and small number of kept states, the states that would actually couple and change the low energy spectrum, are truncated at high energies and not correctly taken into account.

From Fig. 15, one can read off a clear tendency for the calculations including strong truncation effects: correlation effects are overestimated in calculations using small discretization parameters Λ , and possibly, small Λ even lead to an insulating solution. Large discretization parameters, on the other hand, seem to underestimate the correlation effects.

For checking the presented results we have performed some additional test calculations reducing the discretiza-

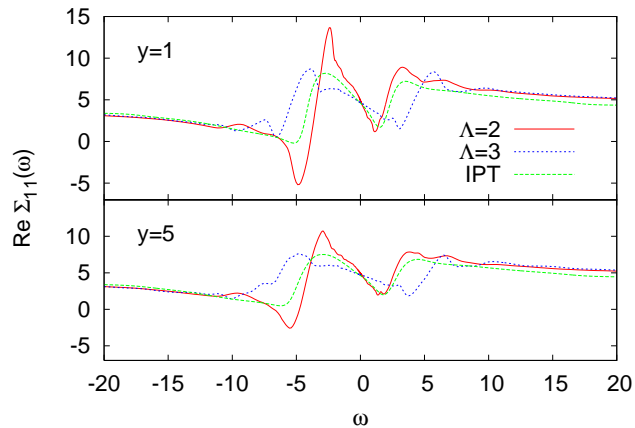


FIG. 16: (Color online) Real part of the self energy for $U = 8$ between two discretization parameters in NRG and IPT as impurity solver. The upper panel shows y -site 1, the lower panel y -site 5.

tion parameter Λ but increasing the number of kept states. Figure 16 shows a comparison for the real part of the selfenergy for $(\Lambda = 3, N_K = 5000)$, $(\Lambda = 2, N_K = 8000)$, and IPT as an impurity solver. The tendency agrees with the results for the one-orbital Hubbard model suffering from the large truncation effects, see Fig. 15. The correlation effects for $\Lambda = 2$ are much more pronounced than for $\Lambda = 3$. The IPT result lies between the two NRG results. Furthermore, increasing the interaction strength using discretization $\Lambda = 2$, leads to a Mott transition at $U \approx 12$. However, in all the calculations using $\Lambda = 2$ we find no signs of edge Mott insulating states and all claims made in the main text remain valid.

- ¹ C. L. Kane and E. J. Mele, Phys. Rev. Lett. **95**, 226801 (2005).
- ² C. L. Kane and E. J. Mele, Phys. Rev. Lett. **95**, 146802 (2005).
- ³ B. A. Bernevig, T. L. Hughes, and S. C. Zhang, Science **314**, 1757 (2006).
- ⁴ B. A. Bernevig and S. C. Zhang, Phys. Rev. Lett. **96**, 106802 (2006).
- ⁵ S. Murakami, Phys. Rev. Lett. **97**, 236805 (2006).
- ⁶ M. König, S. Wiedmann, C. Brüne, A. Roth, H. Buhmann, L. W. Molenkamp, X.-L. Qi, and S.-C. Zhang, Science **318**, 766 (2007).
- ⁷ A. Roth, C. Brüne, H. Buhmann, L. W. Molenkamp, J. Maciejko, X.-L. Qi, and S.-C. Zhang, Science **325**, 294 (2009).
- ⁸ D. Hsieh, D. Qian, L. Wray, Y. Xia, Y. S. Hor, R. J. Cava, and M. Z. Hasan, Nature **452**, 970 (2008).
- ⁹ D. Hsieh, Y. Xia, L. Wray, D. Qian, A. Pal, J. H. Dil, J. Osterwalder, F. Meier, G. Bihlmayer, C. L. Kane, et al., Science **323**, 919 (2009).
- ¹⁰ M. Z. Hasan and C. L. Kane, Rev. Mod. Phys. p. 3045 (2010).
- ¹¹ X. L. Qi and S. C. Zhang, Rev. Mod. Phys. **83**, 1057 (2011).
- ¹² C. Wu, B. A. Bernevig, and S. C. Zhang, Phys. Rev. Lett. **96**, 106401 (2006).
- ¹³ C. Xu and J. E. Moore, Phys. Rev. B **73**, 045322 (2006).
- ¹⁴ A. P. Schnyder, S. Ryu, A. Furusaki, and A. W. W. Ludwig, Phys. Rev. B **78**, 195125 (2008).
- ¹⁵ A. P. Schnyder, S. Ryu, A. Furusaki, and A. W. W. Ludwig, AIP Conf. Proc. **1134**, 10 (2009).
- ¹⁶ A. Kitaev, AIP Conf. Proc. **1134**, 22 (2009).
- ¹⁷ D. Pesin and L. Balents, Nat. Phys. **6**, 376 (2010).
- ¹⁸ V. Gurarie, Phys. Rev. B **83**, 085426 (2011).
- ¹⁹ S. Rachel and K. LeHur, Phys. Rev. B **82**, 075106 (2010).
- ²⁰ M. Hohenadler, T. C. Lang, and F. F. Assaad, Phys. Rev. Lett. **106**, 100403 (2011).
- ²¹ M. Hohenadler and F. F. Assaad (2011), arXiv:1110.3322.
- ²² M. Hohenadler, Z. Y. Meng, T. C. Lang, S. Wessel, A. Muramatsu, and F. F. Assaad (2011), arXiv:1111.3949.
- ²³ Y. Yamaji and M. Imada, Phys. Rev. B **83**, 205122 (2011).
- ²⁴ S. L. Yu, X. C. Xie, and J. X. Li, Phys. Rev. Lett. **107**, 010401 (2011).
- ²⁵ T. Yoshida, S. Fujimoto, and N. Kawakami, arXiv:1111.6250.
- ²⁶ L. Fidkowski and A. Kitaev, Phys. Rev. B **81**, 134509 (2010).
- ²⁷ L. Fidkowski and A. Kitaev, Phys. Rev. B **83**, 075103 (2011).
- ²⁸ A. M. Turner, F. Pollmann, and E. Berg, Phys. Rev. B **83**, 075102 (2011).
- ²⁹ B. Zhou, H. Z. Lu, R. L. Chu, S. Q. Shen, and Q. Niu, Phys. Rev. Lett. **101**, 246807 (2008).
- ³⁰ J. Linder, T. Yokoyama, and A. Sudb (????).
- ³¹ H. Z. Lu, W. Y. Shan, W. Yao, Q. Niu, and S. Q. Shen, Phys. Rev. B **81**, 115407 (2010).
- ³² M. Wada, S. Murakami, F. Freimuth, and G. Bihlmayer, Phys. Rev. B **83**, 121310(R) (2011).
- ³³ C. X. Liu, H. J. Zhang, B. Yan, X. L. Qi, T. Frauenheim, X. Dai, Z. Fang, and S. C. Zhang, Phys. Rev. B **81**, 041307(R) (2010).
- ³⁴ A. C. Potter and P. A. Lee, Phys. Rev. Lett. **105**, 227003 (2010).
- ³⁵ B. Zhou and S. Q. Shen, Phys. Rev. B **84**, 054532 (2011).
- ³⁶ Y. Zhang, K. He, C. Z. Chang, C. L. Song, L. L. Wang, X. Chen, J. F. Jia, Z. Fang, X. Dai, W. Y. Shan, et al., Nat. Phys. **6**, 584 (2010).
- ³⁷ Y. Sakamoto, T. Hirahara, H. Miyazaki, S. I. Kimura, and S. Hasegawa, Phys. Rev. B **81**, 165432 (2010).
- ³⁸ Y. Tanaka and N. Nagaosa, Phys. Rev. Lett. **103**, 166403 (2009).
- ³⁹ C. Y. Hou, E. A. Kim, and C. Chamon, Phys. Rev. Lett. **102**, 076602 (2009).
- ⁴⁰ A. Ström and H. Johannesson, Phys. Rev. Lett. **102**, 096806 (2009).

- ⁴¹ J. C. Y. Teo and C. L. Kane, Phys. Rev. B **79**, 235321 (2009).
- ⁴² A. Georges, G. Kotliar, W. Krauth, and M. J. Rozenberg, Rev. Mod. Phys. **68**, 13 (1996).
- ⁴³ R. Bulla and M. Potthoff, Eur. Phys. J. B **13**, 257 (2000).
- ⁴⁴ M. Potthoff and W. Nolting, Phys. Rev. B **59**, 2549 (1999).
- ⁴⁵ S. Schwieger, M. Potthoff, and W. Nolting, Phys. Rev. B **67**, 165408 (2003).
- ⁴⁶ S. Okamoto and A. J. Millis, Nature **428**, 630 (2004).
- ⁴⁷ S. Okamoto and A. J. Millis, Phys. Rev. B **70**, 241104(R) (2004).
- ⁴⁸ R. W. Helmes, T. A. Costi, and A. Rosch, Phys. Rev. Lett. **101**, 066802 (2008).
- ⁴⁹ H. Zenia, J. K. Freericks, H. R. Krishnamurthy, and T. Pruschke, Phys. Rev. Lett. **103**, 116402 (2009).
- ⁵⁰ R. W. Helmes, T. A. Costi, and A. Rosch, Phys. Rev. Lett. **100**, 056403 (2008).
- ⁵¹ A. Koga, T. Higashiyama, K. Inaba, S. Suga, and N. Kawakami, J. Phys. Soc. Jpn. **77**, 073602 (2008).
- ⁵² A. Koga, T. Higashiyama, K. Inaba, S. Suga, and N. Kawakami, Phys. Rev. A **79**, 013607 (2009).
- ⁵³ E. V. Gorelik, I. Titvinidze, W. Hofstetter, M. Snoek, and N. Blümer, Phys. Rev. Lett. **105**, 065301 (2010).
- ⁵⁴ H. Kajueter and G. Kotliar, Phys. Rev. Lett. **77**, 131 (1996).
- ⁵⁵ T. Saso, J. Phys. Soc. Jpn. **68**, 3941 (1999).
- ⁵⁶ K. Wilson, Rev. Mod. Phys. **47**, 773 (1975).
- ⁵⁷ R. Bulla, T. A. Costi, and T. Pruschke, Rev. Mod. Phys. **80**, 395 (2008).
- ⁵⁸ S. Fujimoto and S. Eggert, Phys. Rev. Lett. **92**, 037206 (2004).
- ⁵⁹ T. Giamarchi, *Quantum Physics in One-Dimension* (Oxford Science Publications, 2004).
- ⁶⁰ A. M. Tsvelik, *Quantum Field Theory in Condensed Matter Physics* (Cambridge University Press, 1995).
- ⁶¹ S. A. Brazovskii and V. M. Yakovenko, Sov. Phys. JETP **62**, 1340 (1985).
- ⁶² V. M. Yakovenko, JETP Lett. **56**, 513 (1992).
- ⁶³ F. V. Kusmartsev, A. Luther, and A. A. Nersesyan, JETP Lett. **55**, 724 (1992).
- ⁶⁴ M. Capone, M. Civelli, S. S. Kancharla, C. Castellani, and G. Kotliar, Phys. Rev. B **69**, 195105 (2004).
- ⁶⁵ M. Sato and S. Fujimoto, Phys. Rev. B **79**, 094504 (2009).
- ⁶⁶ In the context of superconductivity, the odd parity of the local selfenergy $\Sigma_{12,21}(\omega, y)$ corresponds to the anomalous selfenergy of spin-triplet, odd-frequency *s*-wave superconductivity.
- ⁶⁷ G. Moeller, V. Dobrosavljević, and A. E. Ruckenstein, Phys. Rev. B **59**, 6846 (1999).
- ⁶⁸ A. Fuhrmann, D. Heilmann, and H. Monien, Phys. Rev. B **73**, 245118 (2006).
- ⁶⁹ S. S. Kancharla and S. Okamoto, Phys. Rev. B **75**, 193103 (2007).
- ⁷⁰ J. Bauer and A. C. Hewson, Europhys. Lett. **85**, 27001 (2009).
- ⁷¹ J. Bauer, A. C. Hewson, and N. Dupuis, Phys. Rev. B **79**, 214518 (2009).
- ⁷² H. Ishida and A. Liebsch, Phys. Rev. B **82**, 045107 (2010).
- ⁷³ T. Maier, M. Jarrell, T. Pruschke, and H. M. H, Rev. Mod. Phys. **77**, 1027 (2005).
- ⁷⁴ M. Fujita, K. Wakabayashi, K. Nakada, and K. Kusakabe, J. Phys. Soc. Jpn. **65**, 1920 (1996).
- ⁷⁵ D. H. Lee, arXiv:1105.4900.
- ⁷⁶ R. Bulla, Phys. Rev. Lett. **83**, 136 (1999).